Chemical Papers (2023) 77:4245–4264
https://doi.org/10.1007/s11696-023-02774-8

ORIGINAL PAPER

Removal of pharmaceutical compounds from aqueous solution by clay-based synthesized adsorbents: adsorption kinetics and isotherms studies

Mahdieh Azizpourian[1] · Ghazaleh Kouchakzadeh[1] · Zohreh Derikvand[1]

Received: 17 December 2022 / Accepted: 3 March 2023 / Published online: 24 March 2023

Abstract

The presence of pharmaceutical compounds in the environment threatens human health. The introduction of these substances into organic sources causes pollution of plants and soil and creates problems for public health. In this research, the removal of metronidazole and ibuprofen from aqueous solutions was investigated using clay nanocomposites as adsorbents. First, zero-valent iron nanoparticles (nZVIs) were synthesized, and then nZVI-clay and activated carbon-nZVI-clay nanocomposites were prepared. The characteristics of primary materials and synthesized nanocomposites were confirmed by XRD, FT-IR, and SEM techniques. Next, a certain amount of adsorbent was added to different concentrations of drugs separately, and the absorption of the solutions was detected by UV–Vis spectrophotometry at specific times. Afterward, the effects of pH (3–11), adsorbate concentration (10–50 ppm), adsorbent amount (4–12 gL^{-1}), and contact time (15–240 min) were evaluated for the removal of Metronidazole and Ibuprofen. Eventually, the adsorption isotherm and the kinetic behavior of adsorption in an aqueous solution were investigated. The results show that the nanocomposite-activated carbon-nZVI-clay with 20% activated carbon removes 87.11% metronidazole and 87.1% ibuprofen from an aqueous solution at 150 min. The adsorption of drugs on nanocomposites well followed Langmuir adsorption isotherm and pseudo-second-order kinetic model. Overall, it can be concluded that nanotechnology, with the help of natural adsorbents, can offer new solutions in wastewater treatment.

Keywords Fe^0 nanoparticles · Clay · Metronidazole · Ibuprofen · Adsorption

Abbreviations

MNZ	Metronidazole
IBP	Ibuprofen
XRD	X-ray diffraction
SEM	Scanning electron microscope
IR	Infrared
NZVI	Nanoscale zero-valent iron
AC	Activated carbon
10-AC-nZVI-clay	The synthesized nanocomposites with 10%of AC loaded onto clay
20-AC-nZVI-clay	The synthesized nanocomposites with 20% of AC loaded onto clay

Introduction

Clay is a natural material containing several fine-grained minerals (Olive et al. 1989). Since clays have two-dimensional sheets and a size range of 100–1000 nm, they can be named nanoclay. Clay minerals contain silicon (Si) and aluminum (Al) ions that coordinate to oxygen ions and hydroxyl and external ions of structure, which bind to the tetrahedral sheet by one hydroxyl and two oxygen ions (Barton 2002). Nanoclays have various applications regarding their availability, low cost, and low impact on the environment (Guo et al. 2018). The highly available surface area of nanoclay is due to its small size and layered structure (Bergaya et al. 2006). Also, the negative charge of the clay's layered structure is compensated by exchanging cations (Shrivastava et al. 1985). It is expected that the clay surface interacts well with pharmaceutical compounds that possess a positive charge. As these interactions are negligible, clay can be modified and used as a base phase of the nanocomposite. Nanocomposites are multiphase solid materials in which nanoparticles are dispersed into their based phase (Kamigaito et al.

✉ Ghazaleh Kouchakzadeh
gh_kouchakzadeh@yahoo.com

[1] Department of Chemistry, Khorramabad Branch, Islamic Azad University, Khorramabad, Iran

1991). As clay is the oldest ceramic material (Scarre 2005), it can be used as a bulk matrix in the nanocomposite. Clay-based nanocomposites have been used as an adsorbent in many studies (Irandoost et al. 2019; Zhang et al. 2010; Crane et al. 2012; Zhang et al. 2012; Du et al. 2017; Vallet-Regí et al. 1998). Among physical and chemical methods used for contaminants removal, the adsorption technique plays an efficient role because of its convenient efficiency, low cost, and easy operation (Campos et al. 2018; Doğan et al. 2004; Alkan et al. 2007; Kuang et al. 2020). The adsorption phenomenon can also be a good choice for removing pharmaceutical and personal care products from solutions. Pharmaceutical and personal care products are discharged into the environment through wastewater. The pollutants of water resources pose a serious threat to human health and the environment due to the presence of organic matter. Antibiotics and painkillers are organic compounds that are used a lot on a daily basis. (Loos et al. 2013; Cartinella et al. 2006; Nasseh et al. 2019).

Metronidazole (MNZ) is an antibiotic with anti-inflammatory and antibacterial properties. With the commercial name of metronidazole, this antibiotic is 2-methyl-5-nitroimidazole-1-ethanol, and is used in poultry and fish feed as an additive to get rid of parasites (Nasseh et al. 2019; Fang et al. 2011; Momoh et al. 2016). Metronidazole is known as a carcinogen and mutagen substance regarding its chemical composition; therefore, it must be removed from water and wastewater in some way. According to its chemical composition, metronidazole is known as a carcinogenic and mutagenic substance; therefore, it must be removed from water and sewage sources in a way. (Malakootian et al. 2019; Farzadkia et al. 2014; Belhassen et al. 2017).

Ibuprofen (IBP), with the commercial name of ibuprofen, is α-methyl-4-(2-methyl propyl)-benzene acetic acid (Behera et al. 2012; Żółtowska-Aksamitowska et al. 2018; Oba et al. 2021; Nourmoradi et al. 2018; Mondal et al. 2016), is a nonsteroidal and anti-inflammatory drug that is used in the treatment of the rheumatic disorder, fever, and pain (Behera et al. 2012; Żółtowska-Aksamitowska et al. 2018; Oba et al. 2021). Due to Ibuprofen's low metabolism in the body, it is extracted through urine and feces, from where it enters the environment. Previous studies have indicated that ibuprofen and its degraded products can affect the central nervous system and endocrine (Nourmoradi et al. 2018; Mondal et al. 2016; Banerjee et al. 2016).

The release of pharmaceutical compounds into the environment may cause drug resistance in living organisms. Research has shown that MNZ can be removed using various adsorbents like titanium dioxide nanoparticles, biosorbents, nanoscale zero-valent iron nanoparticles, clay, Fe/charcoal, nanocomposites, activated carbon, grapheme, and else adsorbents (Farzadkia et al. 2014; Ighalo et al. 2020; Balarak et al. 2016; Fang et al. 2011; Momoh et al. 2016; Shrivastava et al. 1985; Malakootian et al. 2019; Nasseh et al. 2019; Belhassen et al. 2017; Carrales-Alvarado et al. 2014; Bunmahotama et al. 2020; Carrales-Alvarado et al. 2020; Asgari et al. 2020; Akhtar et al.2016; Ding et al. 2015; Ahmed et al. 2013; Wang et al. 2015; Liu et al. 2017; Hua et al.2018; Nasiri et al. 2022; Ghiasi et al. 2022; Yurtay et al. 2023). Also, chitosan, activated carbon, graphene oxide nanoplatelets, soil mineral, carbon nanotubes, and else adsorbents can be used for IBP removal (Belhassen et al. 2017; Behera et al. 2012; Nourmoradi et al. 2018; Bahamon et al. 2017; Bhadra et al. 2017; Mansouri et al.2015; Guedidi et al. 2017; Banerjee et al. 2016; Cho et al. 2011; Krajišnik et al. 2015; Akhtar et al.2016; de Andrade et al. 2018; Saeid et al. 2018; Oba et al. 2021; Show et al. 2021; Naima et al. 2022; Priyan et al. 2022; Njaramba et al. 2023).

In this research, removal of MNZ and IPB was investigated by clay-based nanocomposites to evaluate adsorption capacity, kinetics behaviors, and the kind of adsorption isotherm. It is worth to say this is the first time that the synthesized nanocomposites with AC loaded onto nZVI-clay were studied to remove metronidazole and ibuprofen from aqueous solution. Furthermore, the effects of adsorption parameters such as initial drug concentration, contact time, adsorbent dose, and solution pH were investigated. The main goal of this work is to provide a method to remove pharmaceutical pollution from the water environment using available adsorbents. In fact, the use of available and affordable absorbents and their good performance can express the importance of this work.

Experimental

Materials

Clay was prepared from the west south of Lorestan province, Iran. Ferric chloride hexahydrate, sodium borohydride, hydrochloric acid, ethanol, sodium hydroxide, and activated carbon were from Merck Company, all of the analytical grades. Metronidazole (Alpha) and Ibuprofen (Sigma-Aldrich) were used as adsorbate. Table 1 shows the structure of used pharmaceutical compounds. All solutions were prepared in distilled water.

Preparation of clay-nanoscale zero-valent iron nanocomposite

Clay-nanoscale zero-valent iron (nZVI) nanocomposite was prepared by synthesizing the nZVI particles. These nanoparticles are produced by various methods, including pulsed laser ablation, chemical vapor deposition, thermal reduction of oxide compounds, thermal decomposition, and aqueous reduction of metallic salts (Crane et al. 2012).

Table 1 Specifications of metronidazole and ibuprofen

Compound	Chemical formula	Chemical structure	Molecular weight ($gmol^{-1}$)	λ_{max} (nm)
Metronidazole	$C_6H_9N_3O_3$	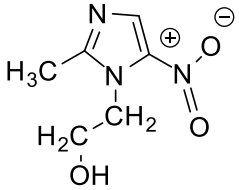	171.15	320
Ibuprofen	$C_{13}H_{17}O_2H$	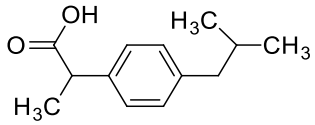	206.00	221

Chemical reduction of ferrous salt is a common method for synthesizing nZVI nanoparticles (Sun et al. 2006). In the present work, Ferric chloride hexahydrate can be reduced by sodium borohydride to produce nZVI. About 50 mL 0.35 M of Fe (III) ion solution was prepared by ferric chloride hexahydrate and ethanol–water mix (30%, v/v). The solution was added to a two-necked flask and stirred under nitrogen gas. Next, 100 mL 1.61 M sodium borohydride was added slowly into the mixture by syringe with a rate of 20–30 drops per minute. The mixture was stirred for 40 min after the addition of all sodium borohydride. Obtaining a black mix can confirm the formation of nZVI nanoparticles. The black solid was separated from the mixture using a strong magnet. Then, the separated solid was washed three times with 5% ethanol to remove rust. The produced solid was vacuum dried overnight (Crane et al. 2012; Sun et al. 2006; Ponder et al. 2000). This synthesis was performed according to Eq. (1) (Sun et al. 2006; Pasinszki et al. 2020):

$$4Fe^{3+} + 3BH_4^- + 9H_2O \rightarrow 4Fe^0 \downarrow + 3H_2BO_3^- + 12H^+ + 6H_2 \uparrow \quad (1)$$

In the next step, nZVI nanoparticles were loaded on clay. Before preparing clay-nZVI, any impurity of nanoclay was removed. The nanoclay was sieved and washed with distilled water and then oven-dried in at 90 ℃ for 12 h. The clay-nZVI nanocomposite was synthesized with two mass contents of nZVI loaded onto the clay. For preparing a 20% mass content of nZVI loaded onto clay, 2 g of clay and 0.5 g nZVI nanoparticles were added to 100 mL ethanol–water (20%, v/v) in a balloon. This balloon was subjected to an ultrasonic (Sonica, Italy) and kept at 80 ℃ for 5 h. Then, the solution was filtered, and the resulting solid was placed in an oven at 80 ℃ for 20 h. The 30% mass content of nZVI loaded onto clay was prepared with the same method and using 0.857 g of nZVI nanoparticles. The synthesized nanocomposites with 20% and 30% nZVI mass contents loaded onto clay were named 20-nZVI-clay and 30-nZVI-clay, respectively.

Preparation of Clay-nZVI-activated Carbon nanocomposite

The 20% mass content of nZVI and 20% mass content of activated carbon loaded onto clay were prepared by adding a certain amount of clay, 3.33 g nZVI nanoparticles, and 3.33 g activated carbon (AC) to 100 mL ethanol–water (20%, v/v) in a round balloon. This balloon was placed into an ultrasonic and kept at 80 ℃ for 5 h. Next, the obtained solid was separated from the liquid phase by filtration and placed in an oven at 80 ℃ for 20 h. The nanocomposite containing 20% mass content of nZVI and 10% mass content of AC loaded onto clay was prepared with the same procedure. The synthesized nanocomposites with 10% and 20% mass contents of AC loaded onto clay were named 10-AC-nZVI-clay and 20-AC-nZVI-clay, respectively.

Preparation of pharmaceutical solutions

A stock solution of 200 mg/L metronidazole and ibuprofen was prepared by dissolving 200 mg of metronidazole in 1 L distilled water (Okhovat et al. 2015; Ramavandi et al. 2015) and ibuprofen in 10% methanol and 90% distilled water in 1 L solution [30–31]. Ibuprofen is soluble in several organic solvents and is less soluble in water (Baccar et al. 2012; Manrique et al. 2007). Several concentrations of metronidazole and ibuprofen solutions were prepared by diluting the stock solution with 10, 20, 30, 40, and 50 ppm for metronidazole, and 10, 20, 30, 40, and 50 ppm for ibuprofen. The wavelengths of maximum absorption of metronidazole and ibuprofen were determined as 320 and 221 nm, respectively, by a UV–Vis spectrophotometer (Perkin-Elmer Lambda 25, USA). A UV–Vis spectrophotometer was used to read absorptions for the wavelengths of maximum absorption and

different concentrations of pharmaceutical solutions. Finally, the concentration calibration curve was drawn for later application (Fig. S1).

Removal of pharmaceutical compounds from aqueous solution

The removal of pharmaceutical compound experiments in contact with the adsorbents was carried out at room temperature (25 ± 1 ℃) on a shaker at 150 rpm (Behsan, Iran). For this purpose, 50-mL Erlenmeyer flasks containing 25 mL of different concentrations of pharmaceutical solutions were used. Optimal conditions of dose of the adsorbents, pH, the concentration of pharmaceutical solutions, and contact time were determined. Residual pharmaceutical compounds concentration in solution after adding a certain amount of adsorbent was measured by taking a sample from the Erlenmeyer flask every 30 min and then centrifuging it for 10 min at 5000 rpm. The absorption of the supernatant was spectrophotometrically read to determine pharmaceutical compounds' concentration in solution. The solution was sampled for 240 min. Eventually, the amount of pharmaceutical compounds adsorbed at equilibrium condition (q_e) and the adsorption capacity of adsorbents at time t (q_t) were calculated using Eq. (2) and Eq. (3) (Żółtowska-Aksamitowska et al. 2018; Nourmoradi et al. 2018; Pap et al. 2020).

$$q_e = \frac{\left(C_i - C_e\right)}{m} V\left(in\ mg\ g^{-1}\right) \tag{2}$$

$$q_t = \frac{\left(C_i - C_t\right)}{m} V\left(in\ mg\ g^{-1}\right) \tag{3}$$

where C_i is initial pharmaceutical compounds concentration (mgL^{-1}), C_e is equilibrium pharmaceutical compounds concentration (mgL^{-1}), m is the weight of the adsorbent (g), and V is solution volume (L). The removal percentage ($R\%$) of pharmaceutical compounds on desired adsorbents was calculated using Eq. (4) (Mondal et al. 2016; Banerjee et al. 2016; Pouretedal et al. 2014).

$$R\% = \frac{\left(C_i - C_e\right)}{C_i} \times 100 \tag{4}$$

The first experiment was to investigate the effect of concentration at different contact times. For this purpose, the samples were taken out from flasks containing different concentrations (10–50 ppm) every 30 min to 240 min. The adsorption almost reached equilibrium condition after around 240 min for all adsorbents. The equilibrium time is the time that the concentration of the pharmaceutical compounds is almost constant. The pharmaceutical compounds' adsorption behavior on the adsorbents' type at the different doses (4–12 gL^{-1}) was studied to evaluate the optimum amount of adsorbent. The effects of pH were investigated using 0.1 M HCl and 0.1 M NaOH for adjusting the desired pH ranges from 3 to 11. All experiments were performed at least in triplicate to ensure the accuracy of the reported data.

Models of adsorption isotherms and kinetics

The adsorption isotherms describe the adsorption process when the amount of adsorbate molecules adsorb on adsorbent at a constant temperature (Foo et al. 2010). The type of isotherm can give helpful information about the nature of adsorption and adsorbents. Equilibrium was reached by evaluating the adsorption through adsorption kinetics experiments (Irandoost et al. 2019). Isotherms like Langmuir and Freundlich were used to describe the adsorption equilibrium process. These experiments were performed using 8 gL^{-1} of synthesized adsorbents in 25 mL drug solution and pH = 7 by different initial concentrations of pharmaceutical compounds: 10, 20, 30, 40, and 50 ppm for 150 min at a constant temperature of 25 ± 1 ℃. Table 2 presents the Langmuir isotherm equation for monolayer adsorption on the adsorbent surface (Langmuir 1918; Baccar et al. 2012). In Table 2, the q_{max} and K_L were calculated from 1/ q_e versus 1/ C_e

Table 2 Linear equations of some of adsorption isotherm models

Isotherm models	Linear equation	Parameters
Langmuir isotherm	$\frac{1}{q_e} = \left(\frac{1}{q_{max}K_L}\right)\frac{1}{C_e} + \frac{1}{q_{max}}$	q_e : the amount of drug adsorbed at equilibrium (mg g^{-1}) q_{max} : the maximum amount of drug adsorbed (mg g^{-1}) K_L : adsorption equilibrium constant (L mg^{-1}) C_e : the equilibrium concentration of drugs in solution (mg L^{-1})
Freundlich isotherm	$Ln\ q_e = Ln\ K_F + \left(\frac{1}{n}\right) LnC_e$	K_F : adsorption capacity n: adsorption intensity

plot. Langmuir adsorption isotherm can be assessed by R_L, which is a dimensionless constant. Also, Eq. (5) was used to estimate the R_L, as follows:

$$R_L = \frac{1}{1 + K_L C_0} \tag{5}$$

where C_0 is the initial adsorbate concentration (mg L^{-1}). The R_L indicates the nature of the adsorption isotherm. If $0 < R_L < 1$, then Langmuir isotherm is favorable. On the other hand, when $R_L = 1$, this isotherm is unfavorable (Mondal et al. 2016).

Table 2 presents Freundlich's empirical isotherm, which is a valid equation for a low concentration of adsorbate solution (Baccar et al. 2012; Walsh et al. 2020). The values of K_F and n are estimated from the diagram of Ln q_e versus Ln C_e (Banerjee et al. 2016).

Linear kinetic models can be used well in the adsorption study, despite their errors. Adsorption kinetics can be used to determine the rate of the compound's removal. The adsorption kinetics is a function of the adsorbent surface, adsorbate concentration, and flow (Pouretedal et al. 2014; Lima et al. 2021). In this study, pseudo-first-order (Lagergren), pseudo-second-order, Elovich, and intra-particle diffusion models (Manjuladevi et al. 2018; Largitte et al. 2016; Edet et al. 2020; Guo et al. 2015; Srivastava et al. 2011; Awad et al. 2020; Hongsawat et al. 2022) were used to investigate the type of adsorption kinetics. The equations of these models are shown in Table 3.

The adsorption kinetics was investigated in specific intervals considering optimal adsorbent dose and pH.

Regeneration of adsorbent

In adsorption process, regeneration of adsorbents is an important item from the economic point of view (Miceli et al. 2021; Gopal et al. 2020). In fact the regeneration process enables the adsorbent surface for reuse. The regeneration functional depends on adsorbent structure, adsorption mechanism, and functional groups (Alsawy et al. 2022). This section was focused on the regeneration of 20-AC-nZVI-clay nanocomposite adsorbent as optimum adsorbent and MNZ drug. The experiments were carried out under optimum conditions of MNZ removal. After the initial adsorption process, the adsorbent was removed by filtration from aqueous solution. The separated adsorbent was washed with deionized water several times and then was dried at 60 °C (Istadi et al. 2016). The 20-AC-nZVI-clay nanocomposite was recycled for three adsorption runs.

Result and discussion

Characterization of synthesis adsorbents

In this research, the synthesized nanocomposites were supported by nanoclay. The XRD pattern of nanoclay samples is presented in Fig. 1a. Using an XRD instrument (Bruker, Germany), this pattern was taken with a Cu-Kα source (λ = 0.154 nm). Soils contain various clay minerals. The nanoclay used in this study contains a large amount of quartz and calcite, and a small amount of montmorillonite, clinochlorite, and illite. The XRD data correspond to the Joint Committee on Powder Diffraction Standards (JCDPS) reference (Zhang et al. 2010; Jiang et al. 2015). The XRD pattern of synthesized nanocomposites is illustrated in Fig. 1b and c. As can be seen, the peak of these nanocomposites is not sharp because they contain a small percentage of activated carbon and nZVI. According to Fig. 1b and c, the peaks corresponding to quartz, calcite, and other minerals are still visible.

Moreover, the diffraction peak at 2θ = 44.9° in Fig. 1b corresponds to the formation of nZVI (Fe^0 state 110) (Zhang et al. 2010; Sun et al. 2006). This result suggests that nZVIs were supported on the clay surface. The broad diffraction peak of carbon (002) can be attributed to the amorphous

Table 3 Linear equations of some of adsorption kinetic models

Kinetic models	Linear equation	Parameters
Pseudo-first-order	$Ln(q_e - q_t) = Ln\, q_e - k_1 t$	q_e : equilibrium adsorption capacity q_t : adsorption capacity at time t k_1 : rate constant
Pseudo-second-order	$\frac{t}{q_t} = \frac{t}{q_e} + \frac{1}{k_2 q_e^2}$	q_e : equilibrium adsorption capacity q_t : adsorption capacity at time t k_2 : rate constant
Elovich	$q_t = \frac{1}{\beta} Ln\,(\alpha\beta) + \frac{1}{\beta} Ln\,(t)$	q_t : adsorption capacity at time t α : initial adsorption rate β : Elovich constant
Intra-particle diffusion	$q_t = k_{dif} t^{0.5} + C$	q_t : adsorption capacity at time t C: a constant that gives about the thickness of the boundary layer k_{dif} : diffusion constant

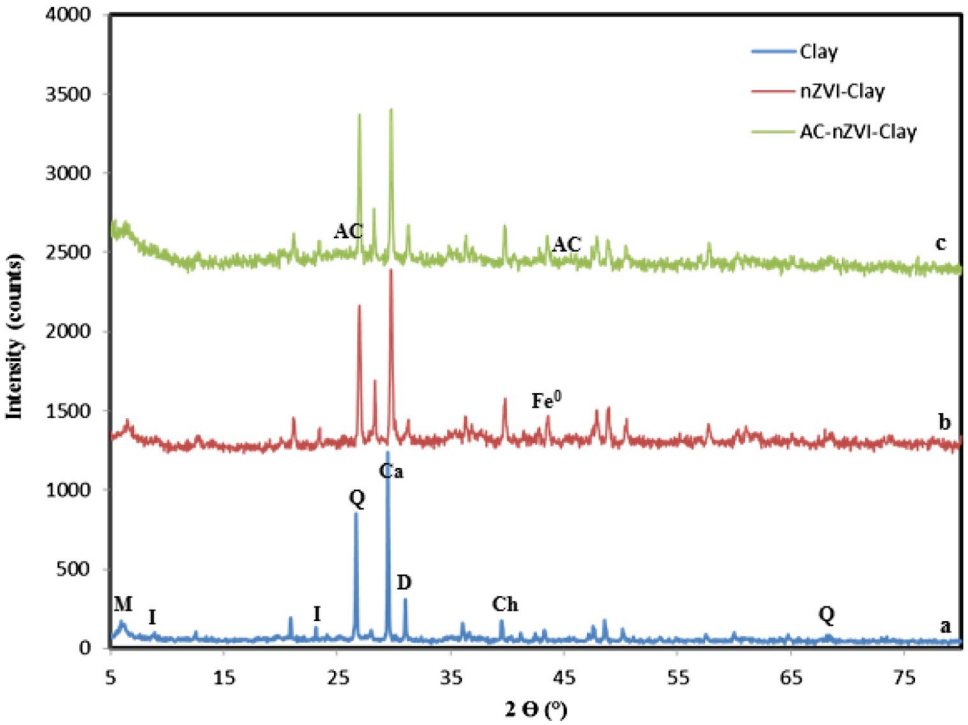

Fig. 1 XRD pattern of **a** Clay, **b** nZVI-Clay nanocomposite, and **c** AC-nZVI-Clay nanocomposite

carbon structure. Therefore, a peak seen about 2θ = 15–25° in Fig. 1c can confirm the presence of activated carbon (Liu et al. 2010; Singh et al. 2014). From Fig. 1, it can be understood that the distance between the plates in the clay structure as a nanocomposite base has not changed because the location of the main peak in the XRD pattern has not changed much. Therefore, it is predicted that nZVI and AC may be adsorbed on the clay surface.

The adsorbents' structures were studied at room temperature by FT-IR spectroscopy. Adsorbents were scanned using Perkin-Elmer Spectrum RXI FT-IR spectrophotometer (USA) through using a KBr pellet in the range of 4000–400 cm^{-1}. Figure 2 shows the FT-IR spectra of clay, nZVI-Clay, and AC-nZVI-Clay. As can be seen from Fig. 2, the FT-IR bands corresponding to clay as the base of nanocomposites have not changed. In other words, after

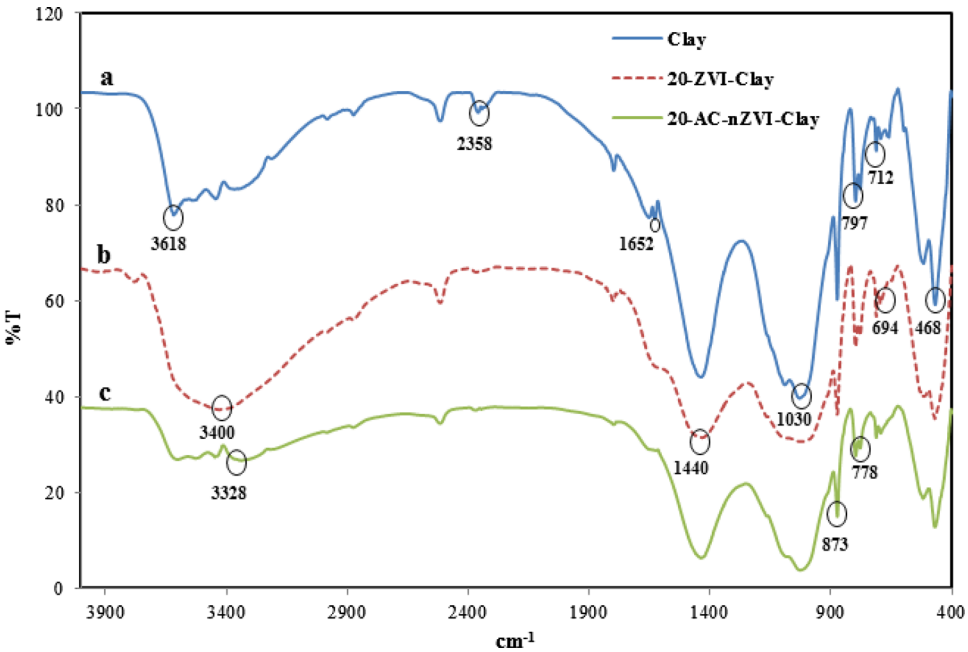

Fig. 2 FT-IR spectra of **a** Clay, **b** AC-nZVI-Clay, and **c** nZVI-Clay

nanocomposites synthesis, the clay structure has been preserved. The bands at about 3300–3650 cm^{-1} correspond to OH stretching vibration elongation. The peaks at 3618 cm^{-1} can be indexed to Al−O−H band in Fig. 2a. Additionally, the band at around 3400 cm^{-1} is slightly broad in Fig. 2c, which can be attributed to Fe^0 (Chen et al. 2011; Castro et al. 2009). The band at 1652 is due to the OH bending vibration of surface-adsorbed H_2O molecule in the clay structure (Zhang et al. 2010; Singh et al. 2011). In addition, the band at around 2358 cm^{-1} can be attributed to atmospheric CO_2 (Rezende et al. 2018). The peaks in the range of 1436–1440 cm^{-1} are due to the stretching vibration of carbonate ions in the clay and nanocomposites spectra. Also, the peak at around 873 cm^{-1} is because of the out-of-plane vibration of carbonate ions (Rodriguez-Blanco et al. 2011; Chen et al. 2005; Frost et al. 2013). Additionally, the band at around 550–700 cm^{-1} suggests the presence of Fe^0 in the nanocomposites spectra. When Fe^0 is added to clay, the peaks of nanocomposites are expected to change relative to the clay. In other words, Si–O and Al–O bonds are partially destroyed by the reaction of $NaBH_4$ and H_2O (Zhang et al. 2010; Abdullah et al. 2018; Xiong et al. 2015; Devi et al. 2016; Mosaleheh et al. 2020). The broad peak at around 1030 cm^{-1} can be indexed to Si–O vibration (Rezende et al. 2018).

The SEM images of adsorbents (i.e., clay, nZVI-clay, and AC-nZVI-clay) in Fig. 3 were used to investigate their morphology. Figure 3a displays clay structure as sheets and glossy layers containing calcite, quartz, and montmorillonite minerals in its structure (Guo et al. 2018; Chen et al. 2011). Similarly, the clay XRD pattern corresponds to the results of its morphology. The nZVI morphology shown in Fig. 3b appears as chain-like and spherical (Chen et al. 2011; Devi et al. 2016). After synthesizing nZVI-clay nanocomposite, Fe^0 nanoparticles were dispersed in clay and were less chain-like (Sun et al. 2006; Chen et al. 2011; Wang et al. 2018). Figure 3c depicts the image of AC-nZVI-clay, which is another nanocomposite used as an adsorbent in this study. As can be seen from this figure, the composite texture has changed compared to previous adsorbents.

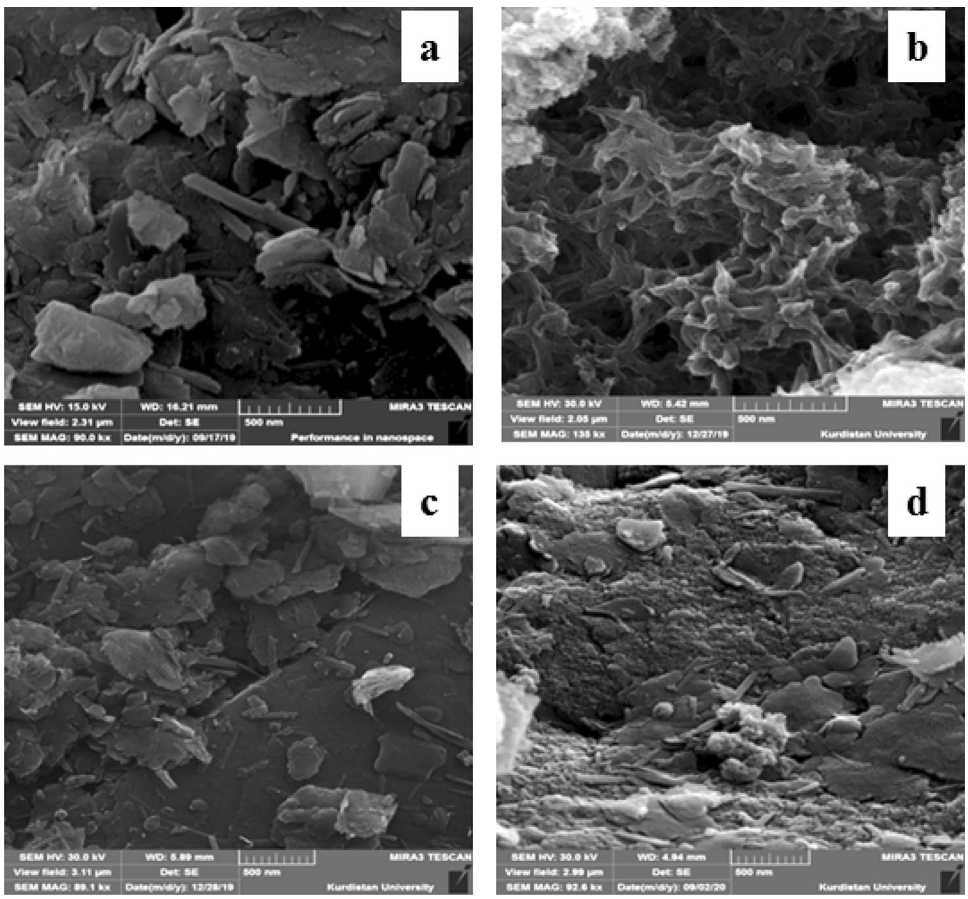

Fig. 3 The SEM images at 500 nm magnification for **a** Clay, **b** nZVI, **c** nZVI-Clay, and **d** AC-nZVI-Clay

Investigating the adsorption of metronidazole and ibuprofen

Effect of the adsorbent type on adsorption

Various experiments indicated that the clay adsorbent was not able to remove metronidazole and ibuprofen. Also, among nZVI-clay nanocomposites, only 20-nZVI-clay could adsorb metronidazole partially, but it did not remove ibuprofen. The absorbent 30-nZVI-clay was not even able to remove these compounds. The clay plates often have a negative electrical charge.

(Das et al. 2016; Moyo et al. 2012), which may repel metronidazole in solution. Table1 shows the specifications of the drugs. Ibuprofen is an organic acid. In this respect, the studies have shown that the clay particles are flocculated in an acidic environment (Shrivastava et al 1985; Rowe et al. 2009). Since the nZVI-clay adsorbent could not remove the pharmaceutical compounds well, a new experiment was performed to ensure that the nZVI adsorbent had removed pharmaceutical compounds. This experiment showed that nZVI could adsorb large amounts of desired pharmaceutical compounds. Therefore, a promising way to solve the problem of low adsorption of nZVI-clay was to add a certain amount of activated carbon to increase the efficiency of the adsorbent. Previous studies (Table 4) have indicated the capability of AC in adsorbing MNZ and IBP from their solutions (Belhassen et al. 2017; Behera et al. 2012; Nourmoradi et al. 2018; Manjunath et al. 2018). The results of the modified nZVI-clay adsorbents with activated carbon indicate an increase in the removal efficiency of the pharmaceutical compounds due to having porosity in the structure of activated carbon (Yuchoong et al. 2013). The results of these experiments and ibuprofen removal efficiency are summarized in Fig. 4.

The present work evaluated the effect of initial concentration and contact time for all adsorbents, including nZVI, nZVI-clay, and AC-nZVI-clay. The main purpose of this research was to study clay-based adsorbents. However, the experiments showed that nZVI-clay nanocomposites do not have good performance in the removal of desired pharmaceutical compounds. Therefore, the adsorbent dose effect, pH effect, evaluation of thermodynamics isotherms, and the kinetic studies were performed only for two AC-nZVI-clay

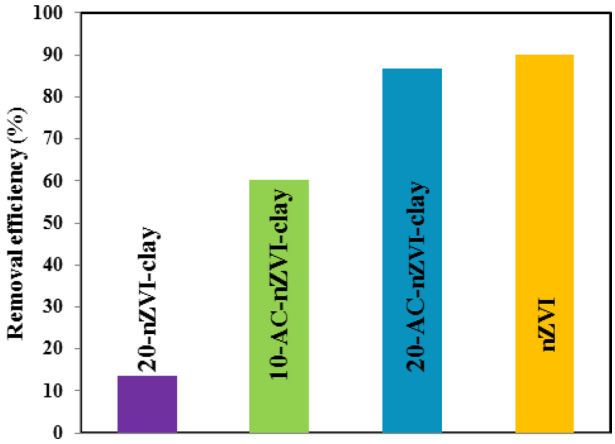

Fig. 4 Effect of different adsorbents on removal percentage of MNZ

adsorbents. In fact, adsorbent-type experiments in this work revealed that the best adsorbents are 10-AC-nZVI-clay and 20-AC-nZVI-clay.

Effect of initial concentration and contact time

After determining the maximum wavelengths and drawing calibration curves, the experiments were performed to show the optimum initial concentration for the maximum removal of pharmaceutical compounds and identify optimum contact time when pharmaceutical solutions reach equilibrium. Figure 5 and the data of Table 5 show the effect of initial concentration and contact time metronidazole solutions on nZVI, nZVI-clay and, AC-nZVI-clay adsorbents. According to Table 5, maximum removal of metronidazole and ibuprofen was performed by nZVI adsorbent and 20-AC-nZVI-clay, respectively. The adsorption of ibuprofen on nZVI adsorbent underperformed compared to metronidazole, probably due to the increased accumulation of ibuprofen molecules on the adsorbent (Fang et al. 2011). As displayed in Fig. 5, the removal amounts of pharmaceutical compounds have increased with increase in concentration. Generally, it can be stated that concentration can influence the driving force (Ramavandi et al. 2015). Also, the drugs were removed better by 20-AC-nZVI-clay adsorbent, probably due to the porosity increase in the adsorbent (Pouretedal

Table 4 The conditions of MNZ and IBP removal by activated carbon in the literature

Compound	%Remove	Concentration (ppm)	Contact time (min)	Adsorbent dose (gL^{-1})	Reference
MNZ	64	50	20	0.5	Belhassen et al. 2017
MNZ	33.8	1	60	1	Manjunath et al. 2018
IBP	100	100	120	5	Nourmoradi et al. 2018
IBP	48	60	360	1	Żółtowska-Aksamitowska et al. 2018

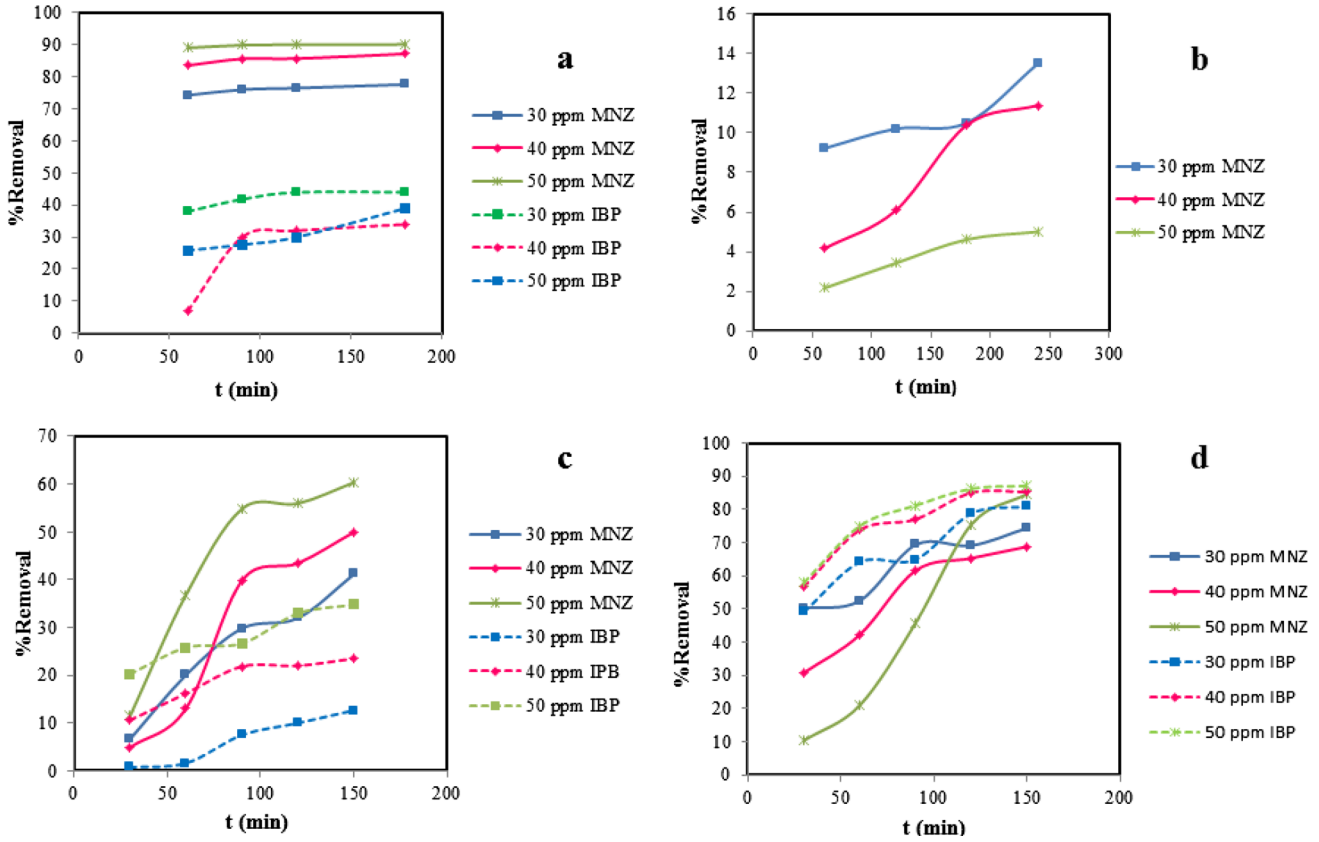

Fig. 5 Influence of contact time and concentration on the removal of MNZ and IBP using **a** nZVI, **b** 20-nZVI-clay, **c** 10-AC-nZVI-clay, and **d** 20-AC-nZVI-clay (adsorbent dose = 8 $gL.^{-1}$, aqueous medium, and temperature = 25 ℃)

Table 5 Comparative results regarding the effect of initial concentration and contact time for different adsorbents (adsorbent dose = 8 gL^{-1}, aqueous medium, and temperature = 25 ℃)

Compound →	Metronidazole			Ibuprofen		
Adsorbent ↓	%Remove	Concentration (ppm)	Contact time (min)	%Remove	Concentration (ppm)	Contact time (min)
nZVI	(90.09)[a] (99.00)[b]	(50)[a] (80)[b]	(180)[a] (49)[b]	44.00	30	180
20-nZVI-clay	13.51	30	240	0	10–50	240
10-AC-nZVI-clay	60.39	50	150	34.78	50	150
20-AC-nZVI-clay	86.63	50	150	87.11	50	150

[a] this work. [b] ref: Fang et al. 2011

et al. 2014). According to Fig. 5, the trend of adsorption in about the first 60–90 min of the process was rapid, exceeding which the adsorption efficiency decreased over time until reaching the equilibrium time.

Effect of adsorbent dose

The effect of the adsorbent dose on adsorption of pharmaceutical compounds was studied by different masses of 10-AC-nZVI-clay and 20-AC-nZVI-clay adsorbents. As shown in Fig. 6, first, the removal of pharmaceutical compounds increased with increase in adsorbents doses. This trend can be attributed to an increase in surface area and access to more adsorbent sites. Also, after a dose of 10 gL^{-1} for MNZ and of 8 gL^{-1} for IBP, the removal efficiency of the pharmaceutical compounds was almost constant, and it seems that active sites of adsorbent are no longer available. The decrease in the removal efficiency after adsorption equilibrium may suggest that the drug molecules have aggregated on adsorbent sites (Pouretedal et al. 2014;

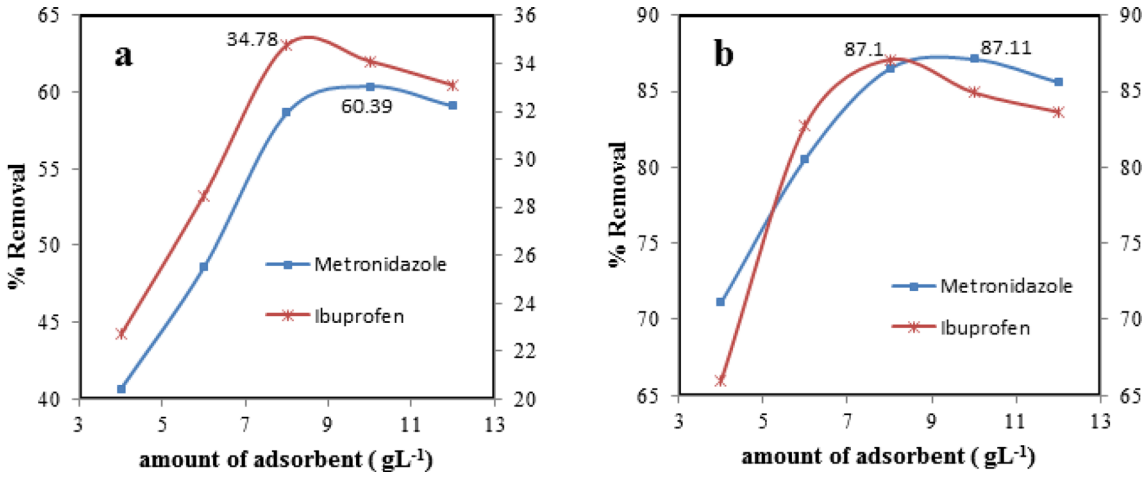

Fig. 6 Effect of adsorbent dose on pharmaceutical compounds removal by **a** 10-AC-nZVI-clay and **b** 20-AC-nZVI-clay adsorbents (drug concentration = 50 ppm, contact time = 150 min, aqueous medium, and temperature = 25 ℃)

Derikvand et al. 2019). The removal efficiency of MNZ and IBP increased from 40.67 to 60.39% and 22.7% to 34.78% on 10-AC-nZVI-clay adsorbent, respectively. In addition, they increased from 71.13% to 87.11% and 66.01% to 87.1% on 20-AC-nZVI-clay adsorbent, respectively.

Effect of pH

The pH is an important parameter that can affect the properties of adsorbents and adsorbates (Tezcanli-Güyer et al. 2004; Bernal et al. 2020). The optimum pH for the removal of MNZ and IBP from their aqueous solution was predicted by investigating different solution pHs ranging from 3 to 11. The removal percentage of MNZ is depicted in Fig. 7. These results represent an increase from 53.36 to 79.14% on 20-AC-nZVI-clay adsorbent when increasing the solution pH from 3 to 5. A further increase in pH leads to a reduction in MNZ removal percentage and an increase in the solution's turbidity. According to previous studies, the pK_a of MNZ is 2.55 (Nasseh et al. 2019; Malakootian et al. 2019). The pH variations can change the charge of the adsorbent surface and MNZ (Nasseh et al. 2019; Carrales et al. 2014). The clay used in this study seems to carry a negative charge on its surface, and cation exchange takes place between the clay interlayers (Du et al. 2017; Nazir et al. 2016). It is noteworthy that clay is flocculated at acidic pH, and it may form a barrier to keep drug diffusion on adsorbent (Shrivastava et al.1985). The clay surface may contain silanol groups,

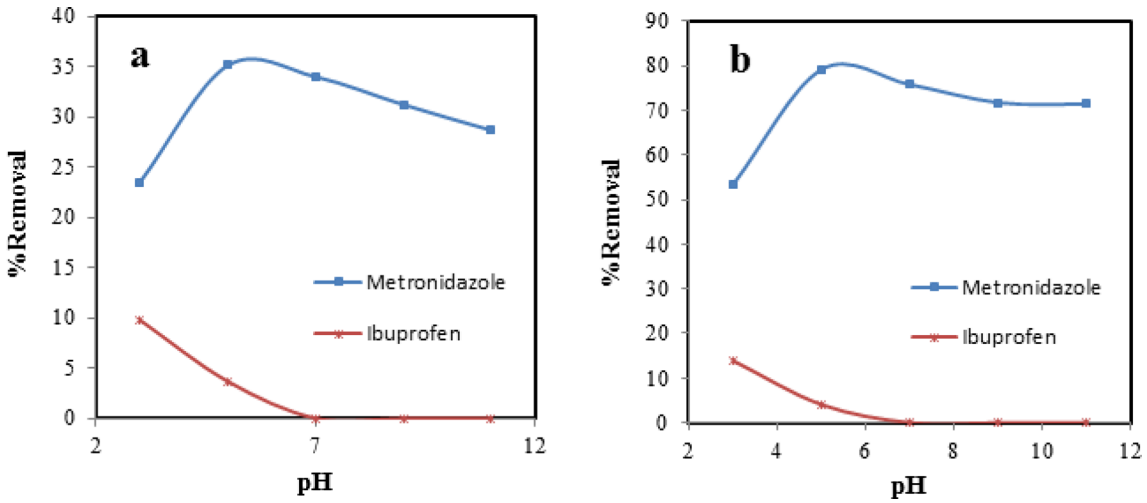

Fig. 7 Effect pH on removal of MNZ and IBP by **a** 10-AC-nZVI-clay and **b** 20-AC-nZVI-clay adsorbents (drug concentration = 50 ppm, contact time = 150 min, pH = 3–11, and temperature = 25 ℃)

which become deprotonated with raising pH solution. Therefore, the number of negative charge sites on nanocomposite increases (Chagas et al. 2014) such that it cannot be favorable for MNZ adsorption in this condition.

MNZ has a positive charge (MNZ-H^+) at acidic conditions (Nasseh et al. 2019; Malakootian et al. 2019; Ramavandi et al. 2015) and seems to be adsorbed on the adsorbent surface at low pHs. In higher pHs, MNZ can possess a negative charge (MNZ-OH^-) (Nasseh et al. 2019). Thus, adsorbent and pharmaceutical compounds repel each other. According to Fig. 7, when pH increases from 5 to 11, MNZ removal decreases from 79.14% to 71.35% on 20-AC-nZVI-clay adsorbent. The obtained results show that the solution contains adsorbent, and MNZ has turbidity at high pH. Any change in pH level affects the adsorbent surface. Similar results were observed for MNZ adsorption on 10-AC-nZVI-clay adsorbent. In this study, nZVI and AC were supported by clay, which is confirmed by the XRD images. At high pH, it seems that the edge charge of clay is neutralized, and its net particle charge is increased. Therefore, clay particles are separated and dispersed (Shrivastava et al.1985; Shah et al. 2009; Chorom et al. 1996), leading to the solution's turbidity. According to obtained results, the optimum necessary pH for the MNZ removal occurs in an aqueous medium. Other studies also indicate that an aqueous medium is an optimum condition for the MNZ removal process (Nasseh et al. 2019; Malakootian et al. 2019; Carrales-Alvarado et al. 2014). In an aqueous medium, nanocomposites (as adsorbent) and MNZ have no repulsion.

The IBP removal was investigated using the AC-nZVI-clay adsorbents. According to previous studies, the pK_a of IBP is 4.9 (Behera et al. 2012; Salim Wahab et al. 2020; Kolawole 2017). When pH increases from 3 to 5, the IBP removal percentage decreases from 13.89% to 4.057%. In higher pHs, IBP is not adsorbed by adsorbents used. Electrostatic interactions are significant in solution, where IBP acidity becomes weak with increasing pH (Behera et al. 2012; Salim Wahab et al. 2020). When pH < pKa, the IBP structure has a molecular state. In addition, if pH > pKa, a carboxylic group in the IBP structure is ionized such that IBP carries a negative charge (Nourmoradi et al. 2018; Méndez-Arriaga et al. 2008). As the number of negative charge sites on nanocomposite increases with raising pH, IBP and used adsorbents repel each other. Therefore, the experiments of IBP adsorption were performed in an aqueous medium. Similar results were observed for IPB adsorption on 10-AC-nZVI-clay adsorbent. Table 6 summarizes the achieved optimum conditions for adsorption of MNZ and IBP on AC-nZVI-clay adsorbents.

By finding out the optimum conditions of adsorption and the removal percentage of desired pharmaceutical compounds in the recent work, the results of this work can be compared with some researches. These results were summarized in Tables 7 and 8.

Adsorption isotherms

Adsorption isotherms were studied using equations shown in Table 2. Figures 8 and 9 present the plot of Langmuir and Freundlich isotherms for adsorption of pharmaceutical compounds on 10-AC-nZVI-clay and 20-AC-nZVI-clay adsorbents, respectively. Tables 9 and 10 display Langmuir and Freundlich's parameters taken from the slope and intercept of the plots. Comparing the value of correlation coefficients revealed that experimental data are in good agreement with Langmuir and Freundlich isotherms equations, although data fitted the Langmuir model more. The Langmuir adsorption model implies monolayer formation and indicates that the active sites on the surface are the same. In contrast, the Freundlich adsorption model indicates that surface site effects are different and related to interactions between functional groups of adsorbent and absorbate molecules (Irandoost et al. 2019). The value of q_{max} in the Langmuir model shows the maximum capacity of adsorption. At MNZ adsorption, by increasing the AC percentage in adsorbent, the available sites and q_{max} increase (Alamgir et al. 2020). However, R_L also rises, suggesting that the adsorption process based on the Langmuir model is not much favorable.

According to Table 10 and comparing the correlation coefficients, IBP experimental data were fitted to the Langmuir model better than the Freundlich model. At IBP adsorption, by enhancing the AC percentage in adsorbent, both q_{max} and R_L decline. It can be assumed that the interaction between adsorbent and drug molecules may be influenced the adsorption process. In the Freundlich equation, parameter n indicates the favorability of the adsorption process.

Table 6 The resulted optimum conditions for pharmaceutical compounds removal on AC-nZVI-clay adsorbents

Experiment	Contact time (min)	pH	Adsorbent dose (g/L)	MNZ concentration (mg/L)	IBP concentration (mg/L)	Temperature (°C)
Effect of contact time	0–240	7	8	10–50	10–50	25 ± 1
Effect of adsorbent dose	(150)[a]	7	4–12	50	50	25 ± 1
Effect of pH	(150)[a]	3–11	8	50	50	25 ± 1

[a] for MNZ and IBP

Table 7 Comparison of MNZ adsorption capacity of this work with other reported

Drug	Adsorbent	Maximum adsorption capacity or removal percentage	References
MNZ	nZVI	90.1%	This work
	20-nZVI-clay	13.51%	This work
	10-Ac-nZVI-clay	60.39%	This work
	20-Ac-nZVI-clay	87.11%	This work
	Biomass-based activated carbon	833 mg/g	Yurtay et al. (2023)
	MIL101-OH/chitosan	600 mg/g	Ghiasi et al. (2022)
	$CoFe_2O_4$ @CMC/HZSM-5 nanocomposite	206.6 mg/g	Nasiri et al. (2022)
	MgO coated clay	84.5 mg/g	Awad et al. (2020)
	Conjugated microporous polymers		Ighalo et al. (2020)
	Fe3O4-chitosan	97.06 mg/g	Asgari et al. (2020)
	Graphene oxide	190 mg/g	Carrales-Alvarado et al. (2020)
	Fe/charcoal	90%	Malakootian et al. (2019)
	FeNi3/SiO2/CuS magnetic nanocomposite	65.15%	Nasseh et al. (2019)
	Biomass carbon foam (BCF- P123)	67.52 mg/g	Hua et al. (2018)
	Granular activated carbon	110.64	Liu et al. (2017)
	Commercial activated carbon (CAC)	328 mg/g	Akhtar et al. (2016)
	Procedure CAC	287 mg/g	Akhtar et al. (2016)
	Activated carbon	144.9 mg/g	Akhtar et al. (2016)
	Carbon spheres-supported nanoscale zero-valent iron	96.79%	Wang et al. (2016)
	FeCl3- induced crude extract	89.3%	Ramavandi et al. (2015)
	Modified sepiolite	36.5%	Ding et al. (2015)
	TiO_2 nanoparticles	99.55%	Okhovat et al. (2015)
	Commercial activated carbon	248.6 mg/g	Carrales-Alvarado et al. (2014)
	Nano-ZnO	96.55%	Farzadkia et al. (2014)
	Activated carbon Siris seed	196.31 mg/g	Ahmed et al. (2013)
	Nanoscale zero-valent iron particles	96.4%	Fang et al. (2011)

When the value of n is larger than 1, the adsorption process is favorable (Buburuzan Haleta et al. 2009). According to Table 9, MNZ removal by 20-AC-nZVI-clay adsorbent has a high favorable correlation with Freundlich equation.

Adsorption kinetics

In this step, the kinetic models of pseudo-first-order, pseudo-second-order, Elovich, and intra-particle diffusion were studied. The adsorption capacity and adsorption condition can be evaluated using adsorption kinetics (Arab et al. 2020; Liu et al. 2021). Tables 11 and 12 show the calculated data in the adsorption of pharmaceutical compounds at different contact times on AC-nZVI-clay adsorbents. Comparing the correlation coefficients of three kinetic models (pseudo-first-order, pseudo-second-order, and Elovich) indicates that adsorption kinetics has a high level of conformity with the pseudo-second-order kinetic model. According to assumptions of adsorption kinetics (Largitte et al. 2016), it seems that pharmaceutical compounds have been adsorbed by the monolayer on the adsorbents, suggesting that the adsorption may be chemisorption. This assumption corresponds to the results of their adsorption thermodynamics. Comparing the correlation coefficients of pseudo-second-order model for two adsorbents (10-AC-nZVI-clay and 20-AC-nZVI-clay) indicates that MNZ was removed by 10-AC-nZVI-clay adsorbent better than other adsorbents. However, for IBP, this trend is the inverse. Figure 10 displays the plots of these three kinetic models. As can be seen, the distance between experimental adsorption capacity ($q_{e,exp}$) and calculated adsorption capacity (q_e) is close to each other in kinetic models for MNZ removal by 10-AC-nZVI-clay and IBP removal by 20-AC-nZVI-clay.

The intra-particle diffusion model was used to evaluate the migration of pharmaceutical compounds from solution to adsorbents surface. The adsorption process involves two steps involving the migration of adsorbates from solution to the adsorbent surface and then intra-particle diffusion of adsorbates into the adsorbent pores [14, 17, 93, 96] (Campos et al. 2018; Kuang et al. 2020; Buburuzan Haleta et al. 2009; Dogan et al. 2006). Figure 11 presents the concentration variation of pharmaceutical compounds as a function

Table 8 Comparison of IBP adsorption capacity of this work with other reported

Drug	Adsorbent	Maximum adsorption capacity or removal percentage	References
IBP	nZVI	43.95%	This work
	20-nZVI-clay	–	This work
	10-Ac-nZVI-clay	34.78%	This work
	20-Ac-nZVI-clay	87.1%	This work
	Gelatin/zirconium-based metal–organic framework	10.23 mg/g	Njaramba et al. (2023)
	Biochar from pepper stems	569.6 mg/g	Naima et al. (2022)
	Corn starch nanoparticles	65.48 mg/g	Priyan et al. (2022)
	Bamboo waste	278.55 mg/g	Show et al. (2021)
	Rice husk	239.8 mg/g	Show et al. (2021)
	Kola nut husk	39.22 mg/g	Show et al. (2021)
	Mesoporous carbon	120 mg/g	Oba et al. (2021)
	Magnetized AC	261.4 mg/g	Oba et al. (2021)
	Microporous activated carbon	495 mg/g	Oba et al. (2021)
	Physically activated coal	430.4 mg/g	Oba et al. (2021)
	bentonite	16.41 mg/g	de Andrade et al. (2018)
	Natural Clay	3.52 mg/g	de Andrade et al. (2018)
	Activated carbon	96.15 mg/g	Nourmoradi et al. (2018)
	Fe-beta zeolite	93%	Saeid et al. (2018)
	Chitin modified with kraft lignin	94.2%	Żółtowska-Aksamitowska et al. (2018)
	Activated carbon	273.87 mg/g	Bahamon et al. 2017
	Metal–organic framework	320 mg/g	Bhadra et al. (2017)
	Activated carbon cloth	491.9 mg/g	Guedidi et al. (2017)
	Activated carbon	145.2 mg/g	Akhtar et al. (2016)
	Graphene oxide nanoplatelets	98.17%	Banerjee et al. (2016)
	Biosorbent (*)	99%	Mondal et al. (2016)
	Modified natural zeolite	19.27 mg/g	Krajišnik et al. (2015)
	Activated carbon	0.29 mg/g	Mansouri et al.(2015)
	Montmorillonite	6.1 mg/g	Behera et al. (2012)
	Activated carbon	10.83 mg/g	Baccar et al. (2012)
	Carbon nanotube	231.5 mg/g	Cho et al. (2011)

(*)Chemically modified N-biochar (N-biochar engineered from precursor Parthenium hysterophorus)

of time (Żółtowska-Aksamitowska et al. 2018; Pouretedal et al. 2014). The plot slope is sharp in the first step, and then it becomes slow and flat until reaching the equilibrium condition. In the first step, the adsorption capacity increases, and it seems that adsorbate molecules transfer from solution toward adsorbent surface well. When the plot of the intra-particle diffusion model passes through the origin, the adsorption process only controls by the diffusion step. Otherwise, it can be controlled with two or three steps (Campos et al. 2018).

In this work, the adsorption process can control by two steps. It seems that the intra-particle diffusion model can predict the adsorption mechanism for MNZ and IBP. According to Fig. 11, the adsorption rate of MNZ increases from the initial time until 60 min on 10-AC-nZVI-clay adsorbent and then becomes slower until reaching equilibrium conditions. In comparison, the adsorption rate of MNZ on 20-AC-nZVI-clay adsorbent increases until 90 min and declines after this time. Evaluating the first step data indicates that the plot of adsorption capacity versus $t^{0.5}$ has a negative intercept, which is the constant C. This constant represents a lag time for the mass transfer migration toward the adsorbent surface (Obradović 2020). Also, it is defined as a constant that gives the thickness of the boundary layer or the boundary layer resistance. With decrease in the boundary layer resistance, the mobility of pharmaceutical compounds increases during the adsorption process (Doğan et al. 2006). The lag times of MNZ molecules for migration toward 10-AC-nZVI-clay and 20-AC-nZVI-clay adsorbents were calculated to be 13 min and 4 min, respectively, indicating that the adsorption

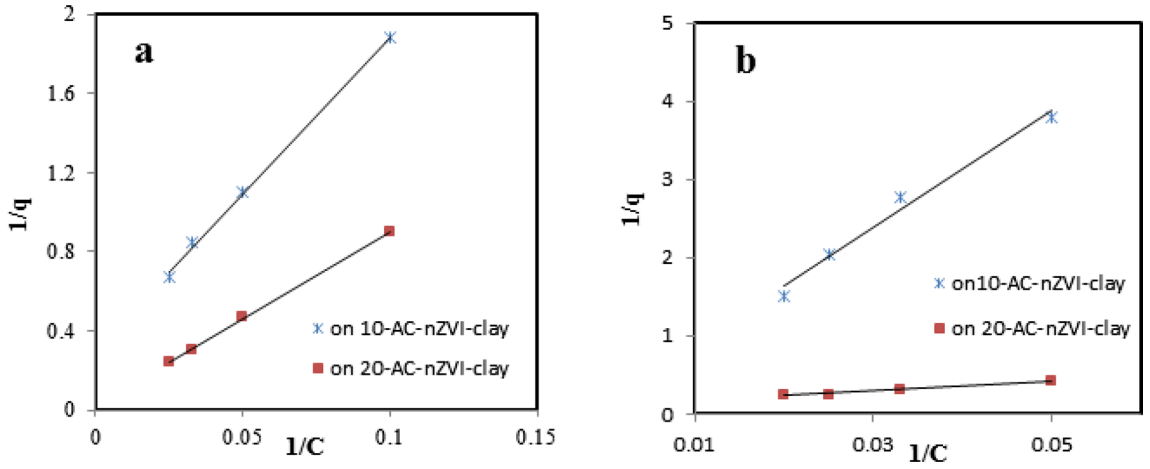

Fig. 8 Plot of Langmuir isotherms for adsorption of **a** MNZ and **b** IBP on 10-AC-nZVI-clay and 20-AC-nZVI-clay adsorbents

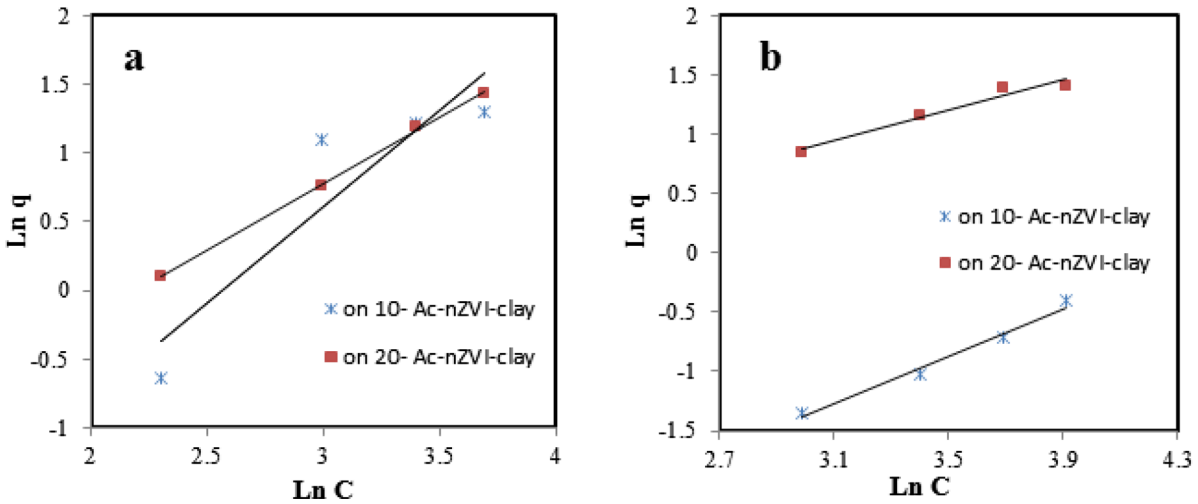

Fig. 9 Plot of Freundlich isotherms for adsorption of **a** MNZ and **b** IBP on 10-AC-nZVI-clay and 20-AC-nZVI-clay adsorbents (drug concentration = 20–50 ppm, contact time = 150 min, aqueous medium, and temperature = 25 ℃)

Table 9 Evaluated parameters for MNZ adsorption isotherms (initial concentration = 20–50 ppm, aqueous medium, temperature = 25 ℃, and contact time = 150 min)

Isotherm models	Parameters	10-Ac-nZVI-clay	20-Ac-nZVI-clay
Langmuir	q_m(mg g^{-1})	3.32	54.35
	K_L(L mg^{-1})	0.019	2.082×10^{-3}
	R_L	0.69	0.95
	R^2	0.998	0.999
Freundlich	K_F	0.027	0.121
	n	0.709	1.04
	R^2	0.846	0.999

Table 10 Evaluated parameters for IBP adsorption isotherms (initial concentration = 20–50 ppm, aqueous medium, temperature = 25 ℃, and contact time = 150 min)

Isotherm models	Parameters	10-Ac-nZVI-clay	20-Ac-nZVI-clay
Langmuir	q_m(mg g^{-1})	7.479	9.737
	K_L(L mg^{-1})	1.78×10^{-3}	0.0159
	R_L	0.93	0.65
	R^2	0.981	0.983
Freundlich	K_F	0.0123	0.349
	n	0. 991	1.55
	R^2	0.983	0.959

Table 11 Parameters evaluated for MNZ adsorption with various kinetic models (initial concentration = 50 ppm, aqueous medium, temperature = 25 ℃, and contact time = 15–150 min)

Kinetic model	Parameters	10-Ac-nZVI-clay	20-Ac-nZVI-clay
Pseudo-first-order	$k_1(\text{min}^{-1})$	0.0265	0.022
	R^2	0.93	0.88
	$q_{e,1}{}^{*}$(mg/g)	1.66	2.43
	$q_{e,exp}{}^{*}$ (mg/g)	2.44	2.90
	Equation	y = − 0.0265x + 0.5051	y = − 0.022x + 0.8872
Pseudo-second-order	$k_2(\text{M}^{-1}\ \text{min}^{-1})$	0.0143	0.0092
	R^2	0.99	0.97
	$q_{e,2}{}^{*}$(mg/g)	1.84	3.45
	$q_{e,exp}{}^{*}$ (mg/g)	2.44	2.90
	Equation	y = 0.5425x + 20.639	y = 0.2895x + 9.0759
Elovich	β	1.77	1.58
	α	0.34	0.38
	R^2	0.87	0.85
Intra-particle diffusion	k_{dif1}	0.2717	0.2347
	C_1	− 0.9794	− 0.4675
	R^2	0.96	0.97
	k_{dif2}	0.0817	0.079
	C_2	0.492	1.122
	R^2	0.98	0.99

Table 12 Parameters evaluated for IBP adsorption with various kinetic models (initial concentration = 50 ppm, aqueous medium, temperature = 25 ℃, and contact time = 15–150 min)

Kinetic model	Parameters	10-Ac-nZVI-clay	20-Ac-nZVI-clay
Pseudo-first-order	$k_1(\text{min}^{-1})$	0.0215	0.0631
	R^2	0.85	0.96
	$q_{e,1}{}^{*}$(mg/g)	2.41	6.91
	$q_{e,exp}{}^{*}$(mg/g)	2.14	4.11
	Equation	y = − 0.0215x + 0.8792	y = − 0.0631x + 1.9326
Pseudo-second-order	$k_2(\text{M}^{-1}\ \text{min}^{-1})$	0.0073	0.0207
	R^2	0.97	0.99
	$q_{e,2}{}^{*}$(mg/g)	2.76	4.53
	$q_{e,exp}{}^{*}$ (mg/g)	2.14	4.11
	Equation	y = 0.3628x + 17.919	y = 0.2211x + 2.363
Elovich	β	1.03	1.41
	α	0.061	2.46
	R^2	0.96	0.82
Intra-particle diffusion	k_{dif1}	0.1844	0.8618
	C_1	− 0.5644	− 2.3432
	R^2	0.97	0.86
	k_{dif2}	0.0771	0.0119
	C_2	0.3794	3.9587
	R^2	0.98	0.99

process is somewhat delayed. The parameters values of the intra-particle diffusion equation for MNZ are represented in Table 11.

According to Fig. 11, the adsorption rate of IBP during 90 min is fast on 10-AC-nZVI-clay adsorbent then slightly decreases. The adsorption rate of IBP on 20-AC-nZVI-clay adsorbent during 60 min is fast, then declines, and becomes roughly constant. These results indicate that the type of drug interaction with adsorbents and the type of adsorbent play a significant role in estimating the adsorption mechanism (Żółtowska-Aksamitowska et al. 2018). Based on the calculations for the first step, the lag time of IBP molecules for migration toward 10-AC-nZVI-clay and 20-AC-nZVI-clay adsorbents was 9.4 min and 7.4 min, respectively. The values

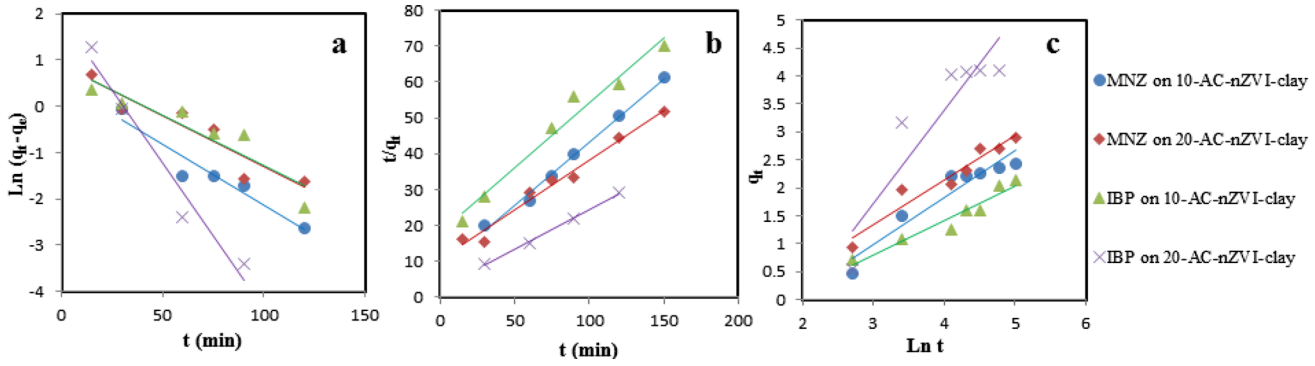

Fig. 10 Plot of kinetic models of MNZ and IBP adsorption on 10-AC-nZVI-clay and 20-AC-nZVI-clay adsorbents: **a** pseudo-first-order, **b** pseudo-second-order, and **c** Elovich models (drug concentration = 50 ppm, contact time = 15–150 min, aqueous medium, and temperature = 25 ℃)

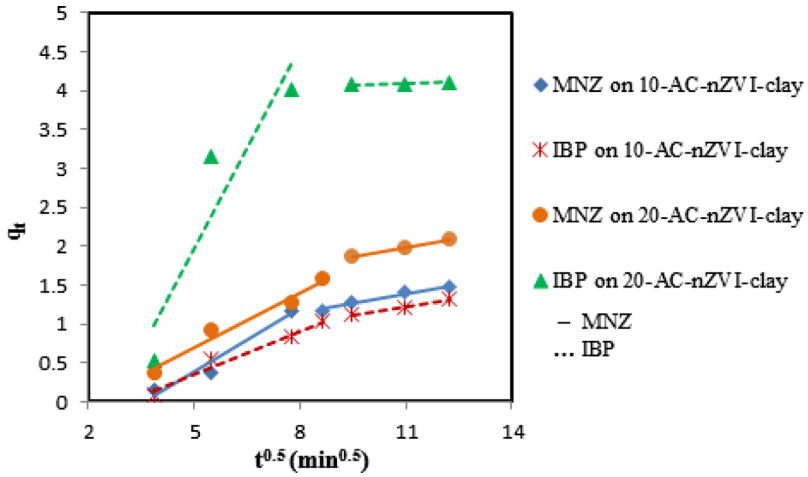

Fig. 11 The plot of the intra-particle diffusion model for MNZ (solid line) and IBP adsorption (dashed line) on 10-AC-nZVI-clay and 20-AC-nZVI-clay adsorbents (drug concentration = 50 ppm, contact time = 15–150 min, aqueous medium, and temperature = 25 ℃)

of the parameters based on intra-particle diffusion equation for IBP are represented in Table 12. As the diffusion parameters change with time, it can conclude that the intra-particle diffusion equation is an approximation for estimation of initial adsorption times (Obradović 2020).

Regeneration and reusability of adsorbent

In order to investigate the regeneration and the reusability of optimum adsorbent, the adsorption process was repeated three runs for adsorption optimum condition of MNZ drug and each time the used adsorbent was regenerated. According to Table 13, the removal efficiency of MNZ after three cycles was decreased from 87.11% to 82.91%. Based on this result, it can state that drug molecules may react with active sites or precipitate on the adsorbent surface and block these sites (Nasiri et al. 2022; Alsawy et al. 2022). After washing and heating adsorbent, some active sites can be nearly regenerated. Next, the stability of the 20-AC-nZVI-clay nanocomposite was investigated with FT-IR spectroscopy study and it showed that the adsorbent was without any notable change (Fig. 12). Therefore, the 20-AC-nZVI-clay nanocomposite can be a suitable adsorbent for the pharmaceutical compounds removal.

Table 13 Removal functional of the MNZ drug from aqueous solution after three recycling cycles at 25 °C and optimum condition

Conditions	Cycle	%Removal
Contact time: 150 min	1	87.11
pH: 7	2	85.65
MNZ Concentration: 50 ppm Adsorbent dose: 10 g/L	3	82.91

Conclusion

The removal of MNZ and IBP is a new application of synthesized clay-based nanocomposites. In this study, the initial adsorption of pharmaceutical compounds was performed using nZVI, nZVI-clay, and AC-nZVI-clay adsorbents. The

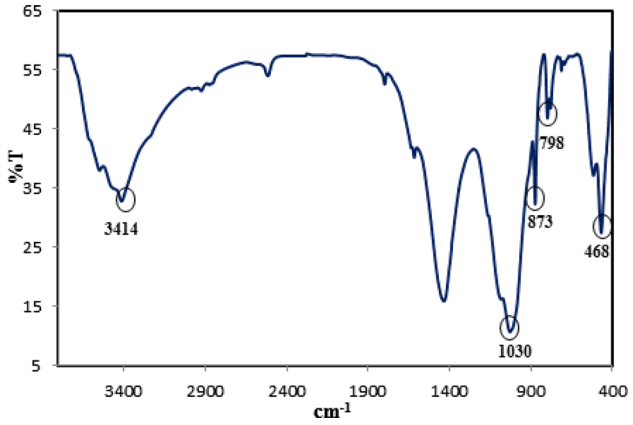

Fig. 12 FT-IR spectra of 20-AC-nZVI-clay nanocomposite after three recycling cycles

experiment results showed that AC-nZVI-clay nanocomposites have a higher ability than other adsorbents clay-based for MNZ and IBP adsorption. Therefore, subsequent experiments were performed by different percentages of AC-nZVI-clay (10-AC-nZVI-clay and 20-AC-nZVI-clay). The optimum conditions for pharmaceutical compounds removal were reported by different experiments, including drug concentration of 50 ppm, contact time of 150 min, and aqueous medium. The results showed that the removal efficiency increases with increase in initial concentration. The optimum dose of adsorbents was 10 gL^{-1} and 8 gL^{-1} AC-nZVI-clay adsorbents for MNZ and IBP, respectively. In these conditions, the removal efficiency of MNZ and IBP was 60.39% and 34.78% on 10-AC-nZVI-clay adsorbent, respectively. Also, it is 87.11% and 87.1% on 20-AC-nZVI-clay adsorbent, respectively. Overall, it can be concluded that IBP is adsorbed with a smaller amount of 20-AC-nZVI-clay adsorbent than MNZ. As a result of evaluations of concentration, pH and adsorbent dose effects and characterization of adsorbents, two factors of π-interactions and electrostatic interaction may be reason for MNZ and IBP adsorption. The adsorption isotherm study showed that desired pharmaceutical compounds' data fit well with the Langmuir isotherm model. A study of the intra-particle diffusion model revealed that adsorption occurred in two steps. The adsorption rate increases until about 60–90 min and declines thereafter. The adsorption process follows the pseudo-second-order kinetic model. Based on the results of this work, it can be claimed that 10-AC-nZVI-clay and 20-AC-nZVI-clay nanocomposites can remove MNZ and IBP from aqueous solution efficiently. It can be concluded that adsorption of MNZ and IBP by the synthesized adsorbents is an effective way to remove pollution. Of course it is predicted that these adsorbents remove other pharmaceutical compounds and organic materials. There are still more good facets of research for this subject.

Supplementary Information The online version contains supplementary material available at https://doi.org/10.1007/s11696-023-02774-8.

Acknowledgements This work was supported by Islamic Azad University, Korramabad Branch.

Declarations

Conflict of interest The authors report no declarations of interest.

References

Aarab N, Hsini A, Essekri A, Laabd M, Lakhmiri R, Albourine A (2020) Removal of an emerging pharmaceutical pollutant (metronidazole) using PPY-PANi copolymer: Kinetics, equilibrium and DFT identification of adsorption mechanism. Groundw Sustain Dev 11:100416

Abdullah B, Ilyas S, Tahir D (2018) Nanocomposites Fe/activated carbon/PVA for microwave absorber: synthesis and characterization. J Nanomater 2018:9823263

Ahmed M, Theydan S (2013) Microporous activated carbon from Siris seed pods by microwave-induced KOH activation for metronidazole adsorption. J Anal Appl Pyrolysis 99:101–109

Akhtar J, Amin NAS, Shahzad K (2016) A review on removal of pharmaceuticals from water by adsorption. Desalin Water Treat 57(27):12842–12860

Alamgir Talha K, Wang B, Liu J-H, Ullah R, Feng F, Yu J, Chen S, Li J-R (2020) Effective adsorption of metronidazole antibiotic from water with a stable Zr(IV)-MOFs: Insights from DFT, kinetics and thermodynamics studies. J Environ Chem Eng 8(1):103642

Alkan M, Demirbas Ö, Doğan M (2007) Adsorption kinetics and thermodynamics of an anionic dye onto sepiolite. Micropor Mesopor Mat 101:388–396

Alsawy T, Rashad E, El-Qelish M, Mohammed RH (2022) A comprehensive review on the chemical regeneration of biochar adsorbent for sustainable wastewater treatment. Npj Clean Water 5:29

Asgari E, Yeganeh SA, J, (2020) Application of the Fe3O4-chitosan nano-adsorbent for the adsorption of metronidazole from wastewater: Optimization, kinetic, thermodynamic and equilibrium studies. Int J Biol Macromol 164:694–706

Awad AM, Jalab R, Benamor A, Nasser MS, Ba-Abbad MM, El-Naas M, Mohammad AW (2020) Adsorption of organic pollutants by nanomaterial-based adsorbents: An overview. J Mol Liq 301:112335

Baccar R, Sarra M, Bouzid J, Feki M, Blanquez P (2012) Removal of pharmaceutical compounds by activated carbon prepared from agricultural by-product. Chem Eng J 211:310–317

Bahamon D, Vega LF (2017) Pharmaceutical removal from water effluents by adsorption on activated carbons: a Monte Carlo simulation study. Langmuir 33(42):11146–11155

Balarak D, Kord Mostafapour F (2016) Canola residual as a biosorbent for antibiotic metronidazole removal. Pharm Chem J 3(2):12–17

Banerjee P, Das P, Zaman A, Das P (2016) Application of graphene oxide nanoplatelets for adsorption of Ibuprofen from aqueous solutions: Evaluation of process kinetics and thermodynamics. Process Saf Environ Prot 101:45–53

Barton CD, (2002) Clay Minerals. In: Rattan Lal, comp, ed. Encyclopedia of Soil Science. New York, New York: Marcel Dekker, pp 187–192.

Behera S, Oh S, Park H (2012) sorptive removal of ibuprofen from water using selected soil minerals and activated carbon. Int J Sci Environ Technol (IJEST) 9(1):85–94

Belhassen H, Ghorbel-Abid I, Rim L (2017) Removal of metronidazole from aqueous solution using activated carbon. Eur J Chem 8(3):310–313

Bergaya F, Lagaly G (2006) Chapter 1 General Introduction: Clays Clay Minerals and Clay Science. Elsevier, Handbook of Clay Science, pp 1–18

Bernal V, Giraldo L, Moreno-Piraján JC (2020) Adsorption of pharmaceutical aromatic pollutants on heat-treated activated carbons: effect of carbonaceous structure and the adsorbent-adsorbate interactions. ACS Omega 5(25):15247–15256

Bhadra BN, Ahmed I, Kim S, Jhung SH (2017) Adsorption removal of ibuprofen and diclofenac from water using metal - organic framework- derived porous carbon. Chem Eng J 314:50–58

Buburuzan Haleta AM, Catrinescu C, Maccoveanu M (2009) Adsorption of n-hexane vapors onto non-functionalized hypercrosslinked polymers (hypersol-macronettm) and activated carbon: equilibrium studies. Environ Eng Manag J 8(1):173–181

Bunmahotama W, Lin TFF, Yang X (2020) Prediction of adsorption capacity for pharmaceuticals, personal care products and endocrine disrupting chemicals onto various adsorbent materials. Chemosphere 238:124658

Campos NF, Barbosa CMBM, Rodríguez-Díaz JM (2018) Removal of naphthenic acids using activated charcoal: kinetic and equilibrium studies. Adsorp Sci Technol 36(7–8):1405–1421

Carrales-Alvarado DH, Ocampo-Pérez R, Leyva-Ramos R, Rivera-Utrilla J (2014) Removal of the antibiotic metronidazole by adsorption on various carbon materials from aqueous phase. J Colloid Interface Sci 436:276–285

Carrales-Alvarado DH, Rodríguez-Ramos I, Leyva-Ramos R, Mendoza-Mendoza E, Villela-Martínez DE (2020) Effect of surface area and physical–chemical properties of graphite and graphene-based materials on their adsorption capacity towards metronidazole and trimethoprim antibiotics in aqueous solution. J Chem Eng 402:126155

Cartinella JL, Cath TY, Flynn MT, Miller GC, Hunter KW, Childress AE (2006) Removal of natural steroid hormones from wastewater using membrane contactor processes. Environ Sci Technol 40:7381–7386

Castro CS, Guerreiro MC, Gonçalves M, Oliveira LCA, Anastácio AS (2009) Activated carbon/iron oxide composites for the removal of atrazine from aqueous medium. J Hazard Mater 164(2):609–614

Chagas NV, Meira JS, Anaissi FJ, Fl M, Quináia SP, Felsner ML, Justi KC (2014) Artigo preparation, characterization of bentonite clay/activated charcoal composites and 2 3 factorial design application in adsorption studies of methylene blue dye. Revista Virtual De Quimica 6(6):1607–1623

Chen ZY, Persson D, Nazarov A, Zakipour S, Thierry D, Leygraf C (2005) In situ studies of the effect of CO[sub 2] on the initial NaCl-induced atmospheric corrosion of copper. J Electrochem Soc 152(9):B342

Chen ZX, Jin XY, Chen Z, Megharaj M, Naidu R (2011) Removal of methyl orange from aqueous solution using bentonite-supported nanoscale zero-valent iron. J Colloid Interface Sci 363(2):601–607

Cho HH, Huang H, Schwab K (2011) Effects of solution chemistry on the adsorption of ibuprofen and triclosan onto carbon nanotubes. Langmuir 27(21):12960–12967

Chorom M (1996) Behaviour of alkaline sodic soils and clays as influenced by pH and Particle charge. Thesis (Ph.D.), University of Adelaide, Dept. of Soil Science.

Crane RA, Scott TB (2012) Nanoscale zero-valent iron: future prospects for an emerging water treatment technology. J Hazard Mater 211–212:112–125

Das MB, Nagaratnam S, Fundamental of Geotechnical Engineering. Fifth edition, Cengage Learning, 2016, pp 1–800.

De Andrade JR, Oliveira MF, da Silva MGC, Vieira MGA (2018) Adsorption of pharmaceuticals from water and wastewater using nonconventional low-cost materials: a review. Ind Eng Chem 57(9):3103–3127

Derikvand Z, Akbari S, Kouchakzadeh G, Azadbakht A, Nemati A (2019) High performance removal of azo and cationic dyes pollutants with Mn-aluminophosphate particles: kinetics, thermodynamics, and adsorption equilibrium studies. Russ J Phys Chem A 93(13):2604–2612

Devi LG, Srinivas M, ArunaKumari ML (2016) Heterogeneous advanced photo- Fenton process using peroxymonosulfate and peroxydisulfate in presence of zero valent metallic iron: a comparative study with hydrogen peroxide photo-Fenton process. J Water Process Eng 13:117–126

Ding H, Bian G (2015) Adsorption of metronidazole in aqueous solution by Fe-modified sepiolite. Desalin Water Treat 55(6):1620–1628

Doğan M, Alkan M, Türkyilmaz A, Ozdemir Y (2004) Kinetics and mechanism of removal of methylene blue by adsorption onto perlite. J Hazard Mater 109(1–3):141–148

Doğan M, Alkan M, Demirbaș Ö, Özdemir Y, Özmetin C (2006) Adsorption kinetics of maxilon blue GRL onto sepiolite from aqueous solutions. Chem Eng J 124:89–101

Du J, Chadalavada S, Naidu R (2017) Synthesis of porous bentonite organoclay granule and its adsorption of tributyltin. App Clay Sci 148:131–137

Edet UA, Ifelebuegu AO (2020) Kinetics, Isotherms, and Thermodynamic Modeling of the Adsorption of Phosphates from Model Wastewater Using Recycled Brick Waste. Process 8(6):865

Fang Z, Chen J, Qiu X, Qiu X, Cheng WEN, Zhu L (2011) Effective removal of antibiotic metronidazole from water by nanoscale zero-valent iron particles. Desalination 268(1–3):8–60

Farzadkia M, Esrafili A, Baghapour MA, Dadban Shahamat Y, Okhovat N (2014) Degradation of metronidazole in aqueous solution by nano-ZnO/UV photocatalytic process. Desalin Water Treat 52:4947–4952

Foo KY, Hameed BH (2010) Insights into the modeling of adsorption isotherm systems. Chem Eng J 156(1):2–10

Frost RL, López A, Scholz R, Xi Y, Belotti FM (2013) Infrared and Raman spectroscopic characterization of the carbonate mineral huanghoite – And in comparison with selected rare earth carbonates. J Mol Struct 1051:221–225

Ghiasi F, Solaimany Nazar AR, Farhadian M, Tangestaninejad Sh, Emami N (2022) Synthesis of aqueous media stable MIL101-OH/chitosan for diphenhydramine and metronidazole adsorption. Environ Sci Pollut Res 29:24286–24297

Gopal RA, Song M, Yang D, Lkhagvaa T, Chandrasekaran S, Choi D (2020) Synthesis of hierarchically structured γ- Fe2O3-PPy nanocomposite as effective adsorbent for cationic dye removal from wastewater. Environ Pollut 267:115498

Guedidi H, Reinert L, Soneda Y, Bellakhal N, Duclaux L (2017) Adsorption of ibuprofen from aqueous solution on chemically surface-modified activated carbon cloths. Arab J Chem 10:S3584–S3594

Guo F, Liu Y, Wang H, Zeng G, Hu X, Zheng B, Li T, Tan X, Wang S, Zhang M (2015) Adsorption behavior of Cr(vi) from aqueous solution onto magnetic graphene oxide functionalized with 1,2-diaminocyclohexanetetraacetic acid. RSC Adv 5(56):45384–45392

Guo F, Aryana S, Han Y, Jiao Y (2018) A review of the synthesis and applications of polymer-nanoclay composites. Appl Sci 8(9):1696

Hongsawat P, Prarat P (2022) Comparative adsorption performance of oxytetracycline and sulfamethoxazole antibiotic on powder activated carbon and grapheme oxide. Chem Pap 76:2293–2305

Hua Z, Wan S, Sun L, Yu Z, Bai X (2018) Role of non-ion surfactants in three-dimensional ordered porous biomass carbon foam derived from the liquefied eucalyptus sawdust for metronidazole adsorption. J Chem Technol Biotechnol 93(10):3044–3055

Ighalo JO, Igwegbe CA, Adeniyi AG, Adeyanju CA, Ogunniyi S (2020) Mitigation of Metronidazole (Flagyl) pollution in aqueous media by adsorption: a review. Environ Technol Rev 9(1):137–148

Irandoost M, Pezeshki-Modaress M, Javanbakht V (2019) Removal of lead from aqueous solution with nanofibrous nanocomposite of polycaprolactone adsorbent modified by nanoclay and nanozeolite. J Water Process Eng 32:100981

Istadi I, Mabruro U, Kalimantini BA, Buchori L, Anggoro DD (2016) Reusability and stability tests of calcium oxide based catalyst (K2O/CaO-ZnO) for transesterification of soybean oil to biodiesel. Bull Chem React Eng 11(1):34–39

Jiang Z, Liu Q, Zhao X, Jin C, Liu C, Li S (2015) Thermal magnetic behaviour of Al-substituted haematite mixed with clay minerals and its geological significance. Geophys J Int 200(1):130–143

Kamigaito O (1991) What Can Be Improved by Nanometer Composites. J Jpn Soc Powder Powder Metall 38:315–321

Kolawole AO (2017) Determination of the affinity of ibuprofen toward aldehyde dehydrogenase by fluorescence quenching. FUTA J Res Sci 13(1):104–112

Krajišnik D, Daković A, Malenović A, Kragović M, Milić J (2015) Ibuprofen sorption and release by modified natural zeolites as prospective drug carriers. Clay Miner 50(1):11–22

Kuang Y, Zhang X, Zhou S (2020) Adsorption of Methylene Blue in Water onto Activated Carbon by Surfactant Modification. Water 12(2):587

Langmuir I (1918) The adsorption of gases on plane surfaces of glass, mica and platinum. J Am Chem Soc 40:1361–1403

Largitte L, Pasquier R (2016) A review of the kinetics adsorption models and their application to the adsorption of lead by an activated carbon. Chem Eng Res Des 109:495–504

Lima EC, Sher F, Guleria A, Saeb MR, Anastopoulos I, Tran HN, Hosseini-Bandegharaei A (2021) Is one performing the treatment data of adsorption kinetics correctly? J Environ Chem Eng 9(2):104813

Liu XY, Huang M, Ma HL, Zhang ZQ, Gao JM, Zhu YL, Han XJ, Guo XY (2010) Preparation of a carbon-based solid acid catalyst by sulfonating activated carbon in a chemical reduction process. Molecules 15(10):7188–7196

Liu P, Wang Q, He ZC, C, (2017) Sorption of Sulfadiazine, Norfloxacin, Metronidazole, and Tetracycline by Granular Activated Carbon: Kinetics, Mechanisms, and Isotherms. Water Air Soil Pollut 228:129

Liu Y, Wang J, Teng W, Hung CT, Zhai Y, Shen D, Li W (2021) Ultrahigh adsorption capacity and kinetics of vertically oriented mesoporous coatings for removal of organic pollutants. Nano Micro Small 17(32):2101363

Loos R, Carvalho R, Antonio DC, Comero S, Locoro G, Tavazzi S, Paracchini B, Ghiani M, Lettieri T, Blaha L, Jarosova B, Voorspoels S, Servaes K, Haglund P, Fick J, Lindberg RH, Schwesig D, Gawlik BM (2013) EU-wide monitoring survey on emerging polar organic contaminants in wastewater treatment plant effluents. Water Res 47:6475–6487

Malakootian M, Kannan K, Gharaghani MA, Dehdarirad A, Nasiri A, Shahamat YD, Mahdizadeh H (2019) Removal of metronidazole from wastewater by Fe/charcoal micro electrolysis fluidized bed reactor. J Environ Chem Eng 7(6):103457

Manjuladevi M, Anitha R, Manonmani S (2018) Kinetic study on adsorption of Cr(VI), Ni(II), Cd(II) and Pb(II) ions from aqueous solutions using activated carbon prepared from Cucumis melo peel. Appl Water Sci 8(1):36

Manjunath SV, Kumar M (2018) Evaluation of single-component and multi-component adsorption of metronidazole, phosphate and nitrate on activated carbon from Prosopıs julıflora. Chem Eng J 346:525–534

Manrique J, Martinez F (2007) Solubility of ibuprofen in some ethanol+watercosolvent mixtures at several temperatures. Lat Am J Pharm 26(3):344–354

Mansouri H, Carmona RJ, Gomis-Berenguer A, Souissi-Najar S, Ouederni A, Ania CO (2015) Competitive adsorption of ibuprofen and amoxicillin mixtures from aqueous solution on activated carbons. J Colloid Interface Sci 449:252–260

Meloun M, Bordovská S, Galla L (2007) The thermodynamic dissociation constants of four non-steroidal anti-inflammatory drugs by the least-squares nonlinear regression of multiwavelength spectrophotometric pH-titration data. J Pharm Biomed Anal 45(4):552–564

Méndez-Arriaga F, Torres-Palma RA, Pétrier C, Esplugas S, Gimenez J, Pulgarin C (2008) Ultrasonic treatment of water contaminated with ibuprofen. Water Res 42(16):4243–4248

Miceli M, Frontera P, Macario A, Malara A (2021) Recovery/reuse of heterogeneous supported spent catalysts. Catal 11(5):591

Momoh M, Ibezim E, Chime S, Adedokun M, Onysih I, Uzondu A, Kabeletoge B, Maduka M (2016) Formulation development and application of natural clay as binder in metronidazole tablets. J Pharm Res Int 13(3):1–9

Mondal S, Aikat K, Halder G (2016) Biosorptive uptake of ibuprofen by chemically modified Parthenium hysterophorus derived biochar: Equilibrium, kinetics, thermodynamics and modeling. Ecol Eng 92:158–172

Mosaleheh N, Sarvi MN (2020) Minimizing the residual antimicrobial activity of tetracycline after adsorption into the montmorillonite: Effect of organic modification. Environ Res 182:109056

Moyo L, Focke WW, Labuschagne FJ, Verryn S (2012) Layered double hydroxide intercalated with sodium dodecyl sulfate. Mol Cryst Liq Cryst 555(1):51–64

Naima A, Ammar F, Abdelkader Q, Rachid C, Lynda H, Syafiuddin A, Boopathy R (2022) Development of a novel and efficient biochar produced from pepper stem for effective ibuprofen removal. Bioresour Technol 347:126685

Nasiri A, Heidari MR, Javid N, Yazdanpanah Gh (2022) New efficient and recyclable magnetic nanohybrid adsorbent for the metronidazole removal from simulated wastewater. J Mater Sci: Mater Electron 33:25103–25126

Nasseh N, Barikbin B, Taghavi L, Nasseri MA (2019) Adsorption of metronidazole antibiotic using a new magnetic nanocomposite from simulated wastewater (isotherm, kinetic and thermodynamic studies). Compos B Eng 159:146–156

Nazir MS, Mohamad Kassim MH, Mohapatra L, Gilani MA, Raza MR, Majeed K (2016) Characteristic Properties of Nanoclays and Characterization of Nanoparticulates and Nanocomposites. In: Jawaid M, Qaiss A, Bouhfid R (eds) Nanoclay Reinforced Polymer Composites, Engineering Materials. Springer, Singapore

Njaramba LK, Kim M, Yea Y, Yoon Y, Park CM (2023) Efficient adsorption of naproxen and ibuprofen by gelatin/zirconium-based metal–organic framework/sepiolite aerogels via synergistic mechanisms. Chem Eng J 452:139426

Nourmoradi H, Moghadam KF, Jafari A, Kamarehie B (2018) Removal of acetaminophen and ibuprofen from aqueous solutions by activated carbon derived from Quercus Brantii (Oak) acorn as a low-cost biosorbent. J Environ Chem Eng 6(6):6807–6815

Oba SN, Ighalo JO, Aniagor CO, Igwegbe CA (2021) Removal of ibuprofen from aqueous media by adsorption: a comprehensive review. Sci Total Environ 780:146608

Obradović B (2020) Guidelines for general adsorption kinetics modeling. Hem Ind 74(1):65–70

Okhovat N, Hashemi M, Golpayegani AA (2015) Photocatalytic decomposition of Metronidazolein aqueous solutions using titanium dioxide nanoparticles. J Mater Environ Sci 6:792–799

Olive WW, Chleborad AF, Frahme CW, Schlocker J, Schneider RR, Schuster RL (1989) Swelling clays map of the conterminous United States. In IMAP. https://doi.org/10.3133/i1940

Pap S, Kirk C, Bremner B, Turk Sekulic M, Shearer L, Gibb SW, Taggart MA (2020) Low-cost chitosan-calcite adsorbent development for potential phosphate removal and recovery from wastewater effluent. Water Res 15(173):115573

Pasinszki T, Krebsz M (2020) Synthesis and application of zero-valent iron nanoparticles in water treatment environmental remediation catalysis and their biological effects. J. Nanomate (basel Switzerland) 10(5):917

Ponder SM, Darab JG, Mallouk TE (2000) Remediation of Cr(VI) and Pb(II) aqueous solutions using supported, nanoscale zero-valent iron. J Environ Sci Technol 34(12):2564–2569

Pouretedal HR, Sadegh N (2014) Effective removal of Amoxicillin, Cephalexin, Tetracycline and Penicillin G from aqueous solutions using activated carbon nanoparticles prepared from vine wood. J Water Process Eng 1:64–73

Priyan V, Narayanasamy S (2022) Effective removal of pharmaceutical contaminants ibuprofen and sulfamethoxazole from water by Corn starch nanoparticles: an ecotoxicological assessment. Environ Toxicol Pharmacol 94:103930

Ramavandi B, Akbarzadeh S (2015) Removal of metronidazole antibiotic from contaminated water using a coagulant extracted from Plantago ovate. Desalin Water Treat 55(8):2221–2228

Rezende JCT, Ramos VHS, Oliveira HA, Oliveira RMPB, Jesus E (2018) Removal of Cr(VI) from aqueous solutions using clay from calumbi geological formation, N. Sra. Socorro, SE State. Brazil Mater Sci Forum 912:1–6

Rodriguez-Blanco JD, Shaw S, Benning LG (2011) The kinetics and mechanisms of amorphous calcium carbonate (ACC) crystallization to calcite, viavaterite. Nanoscale 3(1):265–271

Rowe RC, Sheskey PJ, Quinn ME (2009) Handbook of Pharmaceutical Excipients. Sixth edition, Pharmaceutical Press and American Pharmacists Association.

Saeid S, Tolvanen P, Kumar N, Eränen K, Peltonen J, Peurla M, Mikkola J-P, Franz A, Salmi T (2018) Advanced oxidation process for the removal of ibuprofen from aqueous solution: A non-catalytic and catalytic ozonation study in a semi-batch reactor. Appl Catal B 230:77–90

Salim Wahab H, Mohammed SAM (2020) Removal of ibuprofen residues from acidic aqueous solution by bulk liquid membrane. AIP Conf Proc 2213:020200

Scarre C (2005) The Human Past. Thames and Hudson, London (**0500290636**)

Shah BA, Shah AV, Singh RR (2009) Sorption isotherms and kinetics of chromium uptake from wastewater using natural sorbent material. Int J Environ Sci Technol 6(1):77–90

Show S, Chakraborty P, Karmakar B, Halder G (2021) Sorptive and microbial riddance of micro-pollutant ibuprofen from contaminated water: A state of the art review. Sci Total Environ 786:147327. https://doi.org/10.1016/j.scitotenv.2021.147327

Shrivastava R, Jain SR, Frank SG (1985) Dissolution dialysis studies of metronidazole–montmorillonite adsorbates. J Pharm Sci 74(2):214–216

Singh R, Misra V, Singh RP (2011) Synthesis, characterization and role of zero-valent iron nanoparticle in removal of hexavalent chromium from chromium-spiked soil. J Nanoparticle Res 13(9):4063–4073

Singh P, Raizada P, Kumari S, Kumar A, Pathania D, Thakur P (2014) Solar-Fenton removal of malachite green with novel Fe0-activated carbon nanocomposite. Appl Catal A-Gen 476:9–18

Soo Y, Chada N, Beckner M, Romanos J, Burress J, Pfeifer P (2013–03–20). Adsorbed Methane Film Properties in Nanoporous Carbon Monoliths. Bulletin of the American Physical Society. 58 (1): M38.001. Bibcode: 2013APS..MARM38001S

Srivastava P, Hasan SH (2011) Biomass of mucor heimalis for the biosorption of cadmium frpm aqueous solutions: equilibrium and kinetic studies. BioResources 6(4):3656–3675

Sun YP, Li XQ, Cao J, Zhang WX, Wang HP (2006) Characterization of zero-valent iron nanoparticles. Adv Colloid Interface Sci 120(1–3):47–56

Tezcanli-Güyer G, Ince NH (2004) Individual and combined effects of ultrasound, ozone and UV irradiation: a case study with textile dyes. Ultrasonics 42(1–9):603–609

Vallet-Regí M, Granado S, Arcos D, Gordo M, Cabañas MV, Ragel CV, Salinas AJ, Doadrio AL, Sam Román J (1998) Preparation, characterization, and in vitro release of ibuprofen from AI2O3/PLA/PMMA composites. J Biomed Mater Res 39(3):423–428

Verryn, (2012) Layered double hydroxide intercalated with sodium dodecyl sulfate. Mol Cryst Liq Cryst 555(1):51–64

Walsh K, Mayer S, Rehmann D, Hofmann T, Glas K (2020) Equilibrium data and its analysis with the Freundlich model in the adsorption of arsenic(V) on granular ferric hydroxide. Sep Purif Technol 243:116704

Wang X, Du Y, Liu H, Ma J (2016) Novel synthesis of carbon spheres supported nanoscale zero-valent iron for removal of metronidazole. Appl Surf Sci 390:50–59

Wang X, Du Y, Liu H, Ma J (2018) Ascorbic acid/Fe0 composites as an effective persulfate activator for improving the degradation of rhodamine B. RSC Adv 8(23):12791–12798

Xiong Z, Lai B, Yang P, Zhou Y, Wang J, Fang S (2015) Comparative study on the reactivity of Fe/Cu bimetallic particles and zero valent iron (ZVI) under different conditions of N2, air or without aeration. J Hazard Mater 297:261–268

Yurtay A, Kılıç M (2023) Biomass-based activated carbon by flash heating as a novel preparation route and its application in high efficiency adsorption of metronidazole. Diam Relat Mater 131:109603

Zhang X, Lin S, Lu XQ, Chen Z (2010) Removal of Pb(II) from water using synthesized kaolin supported nanoscale zero-valent iron. Chem Eng J 163(3):243–248

Zhang X, Lin S, Chen Z, Megharaj M, Naidu R (2011) Kaolinite-supported nanoscale zero-valent iron for removal of Pb^{2+} from aqueous solution: reactivity, characterization and mechanism. Water Res 45(11):3481–3488

Żółtowska-Aksamitowska S, Bartczak P, Zembrzuska J, Jesionowski T (2018) Removal of hazardous non-steroidal anti-inflammatory drugs from aqueous solutions by biosorbent based on chitin and lignin. Sci Total Environ 612:1223–1233